Paleoceanography and Paleoclimatology

AGU ADVANCING EARTH AND SPACE SCIENCES

RESEARCH ARTICLE
10.1029/2024PA004892

Oceanography of the Eastern Equatorial Pacific Ocean Across the Oligocene-Miocene Transition

Diederik Liebrand[1,2], Bridget S. Wade[3], Helen M. Beddow[4,5], David J. King[3], Alexander D. Harrison[6], Heather J. H. Johnstone[7], Anna Joy Drury[3,8], Heiko Pälike[7], Appy Sluijs[4], and Lucas J. Lourens[4]

[1]Department of Earth and Environmental Sciences, The University of Manchester, Manchester, UK, [2]PalaeoClimate. Science, Mirfield, UK, [3]Department of Earth Sciences, University College London, London, UK, [4]Department of Earth Sciences, Faculty of Geosciences, Utrecht University, Utrecht, The Netherlands, [5]Now at Global Canopy, Cambridge, UK, [6]School of Earth and Environment, University of Leeds, Leeds, UK, [7]MARUM—Center for Marine Environmental Science, University of Bremen, Bremen, Germany, [8]School of Geography, Geology, and the Environment, University of Leicester, Leicester, UK

Key Points:

- Positive trends mark Oligo-Miocene planktonic and benthic foraminiferal oxygen and carbon isotope records from the east Pacific Ocean
- Surface currents and oceanic exchange through the Central American Seaway influenced surface ocean salinity
- Eccentricity-paced primary productivity variability determined strength of the biological carbon pump

Correspondence to:
D. Liebrand,
diederik@palaeoclimate.science

Citation:
Liebrand, D., Wade, B. S., Beddow, H. M., King, D. J., Harrison, A. D., Johnstone, H. J. H., et al. (2024). Oceanography of the eastern equatorial Pacific Ocean across the Oligocene-Miocene Transition. *Paleoceanography and Paleoclimatology*, *39*, e2024PA004892. https://doi.org/10.1029/2024PA004892

Received 7 MAR 2024
Accepted 15 JUN 2024

Author Contributions:
Conceptualization: Bridget S. Wade, Helen M. Beddow, Heiko Pälike, Appy Sluijs, Lucas J. Lourens
Data curation: Diederik Liebrand, Helen M. Beddow
Formal analysis: Bridget S. Wade, Helen M. Beddow, David J. King, Alexander D. Harrison
Funding acquisition: Bridget S. Wade, Lucas J. Lourens
Investigation: Diederik Liebrand, Bridget S. Wade, Helen M. Beddow, David J. King, Alexander D. Harrison
Methodology: Bridget S. Wade, Helen M. Beddow, David J. King, Alexander D. Harrison
Project administration: Lucas J. Lourens
Resources: Bridget S. Wade, Lucas J. Lourens
Software: Diederik Liebrand, Heather J. H. Johnstone
Supervision: Bridget S. Wade, Appy Sluijs, Lucas J. Lourens

Abstract The functioning of the Pacific Ocean—the world's largest ocean—during a warmer-than-present paleoclimate state remains underexplored. We present planktonic and benthic foraminiferal stable oxygen ($\delta^{18}O$) and carbon ($\delta^{13}C$) isotope records from Integrated Ocean Drilling Program (IODP) Site U1334 that span the Oligocene-Miocene Transition (OMT) interval, from 24.15 to 21.95 million years ago (Ma). We reconstruct (sub-)surface and deep-water conditions and provide better constraints on the physical and chemical oceanography of the eastern equatorial Pacific Ocean (EEP). Positive trends in planktonic and benthic foraminiferal $\delta^{18}O$ values, mark a largely uniform imprint of increased land-ice volume/global cooling on surface- and deep-waters. We document a delayed planktonic foraminiferal $\delta^{18}O$ increase across the OMT as well as an increase in the amplitude variability of planktonic foraminiferal $\delta^{18}O$ values on eccentricity timescales during the early Miocene. We interpret this as an enhanced glacioeustatic sea-level control on Atlantic-Pacific salinity exchange through the Central American Seaway (CAS) or as the onset of more variable surface currents and oceanic fronts in the EEP. Positive trends in planktonic and benthic foraminiferal $\delta^{13}C$ values characterize the whole-ocean depletion in ^{12}C linked to organic carbon burial during the Oligocene-Miocene carbon maximum (CM-OM). However, this depletion is more pronounced in the planktonic foraminiferal $\delta^{13}C$ record, especially during ~400 Kyr eccentricity minima, reflecting an increase in nutrient upwelling and the efficacy of the biological carbon pump (BCP) when global temperatures decreased across the OMT and during the early Miocene. Our study highlights the dynamic behavior of the EEP in a warmer-than-present unipolar icehouse state.

Plain Language Summary Twenty-three million years ago, climatic conditions on Earth were warmer than today, there was a large ice sheet on Antarctica, but, unlike today, not on Greenland. Furthermore, the Atlantic and Pacific Oceans were still connected with a seaway that ran in-between North and South America. This seaway governed the equatorial transport of heat, salt, and nutrients between the two oceans. To better understand the role of the eastern Pacific Ocean in causing and responding to climatic change at this time, we analyzed the chemical composition of foraminifera shells, single celled organisms that lived in the surface and deep waters and at the seafloor. By comparing surface- to deep-water chemistry results, namely oxygen and carbon isotopes, we attempt to reconstruct the chemical and physical structure of the water column. We interpret that the eastern Pacific surface ocean was saltier at times when Atlantic waters were flowing westward. Furthermore, we find an increase in productivity in the equatorial Pacific surface ocean when climate cooled.

1. Introduction

1.1. Scope and Objective of This Study

In this study, we aim to reconstruct oceanographic conditions of the eastern equatorial Pacific Ocean (EEP) during a two million-year-long Oligocene-Miocene Transition (OMT) spanning time interval, from 24.15 to 21.95 million years ago (Ma). The OMT is a time of major Cenozoic climatic change. Detailed benthic foraminifera oxygen and carbon isotope records across the OMT (~23 Ma) reveal marked temperature shifts, ice volume fluctuations and carbon cycle reorganizations (Diester-Haass et al., 2011; Greenop et al., 2019; Kim &

Validation: Diederik Liebrand, Bridget S. Wade, Helen M. Beddow, David J. King
Visualization: Diederik Liebrand, Bridget S. Wade, Helen M. Beddow, David J. King, Heather J. H. Johnstone
Writing – original draft: Diederik Liebrand, Bridget S. Wade, Helen M. Beddow
Writing – review & editing: Diederik Liebrand, Bridget S. Wade, Helen M. Beddow, David J. King, Alexander D. Harrison, Heather J. H. Johnstone, Anna Joy Drury, Heiko Pälike, Appy Sluijs, Lucas J. Lourens

Zhang, 2022; Lear et al., 2004; Liebrand et al., 2017; Mawbey & Lear, 2013). However, to date there have been no high-resolution planktonic foraminifera stable isotope records. Here we present planktonic foraminiferal accumulation rates (PFAR), and stable oxygen and carbon isotope (i.e., $\delta^{18}O$ and $\delta^{13}C$, respectively) records from Integrated Ocean Drilling Program (IODP) Site U1334 (Beddow, 2016). We compare these planktonic data to previously published epifaunal and infaunal benthic foraminiferal $\delta^{18}O$ and $\delta^{13}C$ values, also from Site U1334 (Beddow et al., 2016, 2018), and present isotopic trends and vertical/water column gradients. We examine the timing of upper water column changes and investigate whether the pronounced changes in the benthic foraminifera records are reflected in the tropical Pacific surface ocean. We use these combined data sets to shed new light on the dynamic oceanography of the EEP, and on global climatic, cryospheric, and carbon cycle dynamics, across the OMT. We are especially interested in the potential effects of glacio-eustatic sea level changes on Central American Seaway (CAS) throughflow and surface EEP oceanography. Furthermore, we aim to further constrain the evolution of the biological carbon pump (BCP) in the EEP in response to global cooling across the OMT and across the Oligocene-Miocene carbon maximum (CM-OM) (Hodell & Woodruff, 1994).

1.2. Oligo-Miocene Climatic, Cryospheric, and Geographic Background Conditions

Following the establishment of a continental-sized ice sheet on Antarctica, during the Eocene-Oligocene Transition (EOT) at ~34 Ma, Earth's Oligocene climate-cryosphere system was marked by a highly dynamic evolution, on both astronomical and longer time scales (Liebrand et al., 2017; Pälike, Norris, et al., 2006; Wade & Palike, 2004; Westerhold et al., 2020). High resolution benthic foraminiferal $\delta^{18}O$ records from both the Atlantic and Pacific Oceans detail the evolution of deep-sea (i.e., high latitude, where deep waters sink) temperatures and global ice volumes combined (Beddow et al., 2016; Billups et al., 2002; Liebrand et al., 2016; Pälike, Frazier, et al., 2006). The OMT (at ~23 Ma) interrupts the late Oligocene warming (LOW, i.e., 26.3–23.7 Ma) (Beddow et al., 2016; Liebrand et al., 2017; Zachos et al., 2001), and is marked by a transient ~1.0‰ increase in benthic foraminiferal $\delta^{18}O$ values. The OMT is interpreted as a major global cooling event and probably constitutes a complete re-glaciation of Antarctica following the ice-freer conditions that marked the LOW (Liebrand et al., 2017; Pälike, Norris, et al., 2006). The northern hemisphere (NH) is thought to have remained largely land-ice free during this time, although a relatively short-lived glaciation concurrent with peak OMT conditions cannot be ruled out (DeConto et al., 2008). NH cooling across the OMT probably affected the intensity of El Niño-Southern Oscillation (ENSO) (McPhaden et al., 2006), and is understood to have caused a more permanent southward shift of the intertropical convergence zone in the EEP (Hyeong et al., 2014).

In benthic foraminiferal $\delta^{18}O$ records, the recovery phase of the OMT to near pre-excursion values is characterized by three well-expressed ~110-Kyr cycles (Liebrand et al., 2017; Zachos et al., 2001). In benthic foraminiferal $\delta^{13}C$ records, the OMT interval is associated with the CM-OM (Hodell & Woodruff, 1994), which constitutes a global carbon cycle event marked by a ~1.5-Myr long positive excursion in $\delta^{13}C$ that probably involved the (temporary) storage of biologically fixed ^{12}C on land or on the continental shelves (in North America and South Africa), where organic carbon and phosphate rich deposits of Oligo-Miocene age have been reported (Compton et al., 1990, 1993, 2004; Hodell & Woodruff, 1994; Steinthorsdottir et al., 2021). Shorter-lived and transient carbon cycle perturbations associated with the OMT are also reported from the deep ocean (Diester-Haass et al., 2011; Kim & Zhang, 2022; Mawbey & Lear, 2013). Atmospheric CO_2 concentrations varied broadly between ~450 and ~850 parts per million, with the largest rise in CO_2 values occurring during the early Miocene, after the peak glacial conditions of the OMT (Greenop et al., 2019; Rae et al., 2021). Geographically, Earth looked broadly like the present-day (Steinthorsdottir et al., 2021). However, at ~23 Ma, the Pacific Ocean was wider by about 1,000 km, at the expense of the Atlantic Ocean (Cande & Kent, 1992). Furthermore, the CAS formed either one, or several, deep- and/or shallow-water connection(s) between the Atlantic and Pacific Oceans (Müller et al., 2018).

1.3. Oceanography of the Modern Eastern Equatorial Pacific Ocean

To provide context to our paleoceanographic reconstructions of the EEP, it is important to understand its modern oceanography. The present-day EEP is marked by a complex oceanography with North-South divergent equatorial upwelling, as well as spatially and temporally varying oceanic fronts that impact temperature, salinity, and nutrient-availability (Figures 1 and 2). ENSO variability strongly affects the spatiotemporal heterogeneity of both physical and chemical oceanographic conditions in the modern EEP (McPhaden et al., 2006). Thermocline, pycnocline, nutriclines, and oxycline are situated between ~50 and 200 m water depth (Figure 2) (Boyer

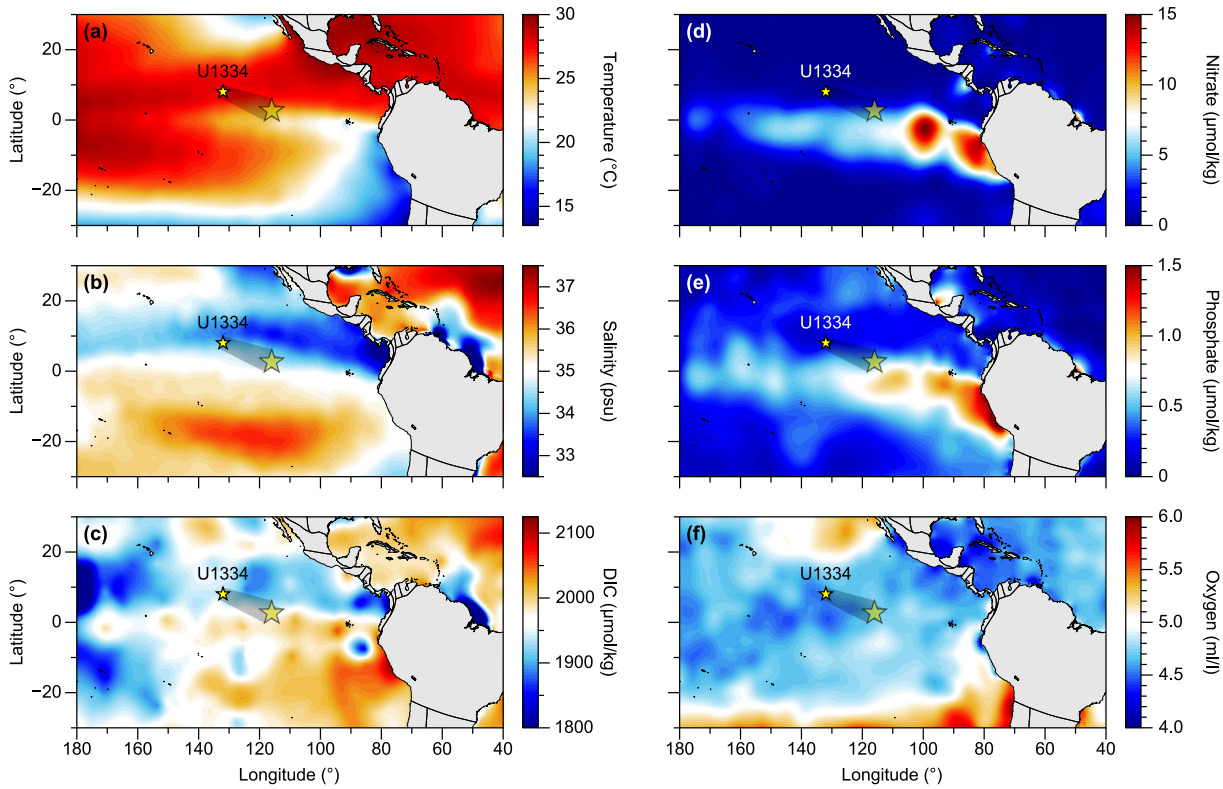

Figure 1. Present-day surface oceanographic context of the EEP. Sea surface (a) temperature, (b) salinity, (c) dissolved inorganic carbon (DIC), (d) nitrate, (e) phosphate, and (f) oxygen (Boyer et al., 2018; Lauvset et al., 2022; Schlitzer, 2022). Present-day location of Site U1334 is indicated with a small full color yellow star (7°59′N, −131°58′W). This location is several degrees to the NW from its paleo-location at 23 Ma (3°N, −116°W) (Pälike et al., 2010) during the OMT, indicated with a large shaded yellow star.

et al., 2018; Lauvset et al., 2022; Schlitzer, 2022). They mark the distinction between the equatorial undercurrent (EUC) and equatorial Pacific intermediate water (EqPIW), on top, and Pacific Deep Water (PDW), below. A combination of Antarctic Bottom Water (AABW) and Circumpolar Deep Water (CDW) is present at depth (Figure 2) (Rippert et al., 2017). However, these deep-water masses are less clearly identifiable in thermocline, pycnocline, and nutriclines, but best expressed in the higher oxygen levels below ∼2 km water depth, especially compared to the near oxygen-depleted values associated with the oxygen minimum zone (i.e., between ∼100 m and ∼1 km water depth, Figure 2). The EEP is currently a net source of carbon dioxide (CO_2) to the atmosphere, because wind-driven equatorial upwelling and advection of relatively old, deep, Southern Ocean-sourced, and CO_2-rich waters lead to a regionally high surface-ocean partial pressure of dissolved CO_2 compared to CO_2 in the atmosphere, and hence, to high rates of sea-to-air gas exchange (Feely et al., 1999; Takahashi et al., 2002). This process thus constitutes an important flux within the present-day exogenic carbon pool. At the same time, upwelling lowers surface ocean temperatures, creating the so-called "cold tongue" (Wyrtki, 1981): a region of cool sea surface temperatures in the EEP (Figure 1) (Schmitz Jr., 1995; Toggweiler et al., 1991; Wyrtki, 1981). Furthermore, equatorial upwelling increases regional nutrient availability and primary productivity, best evidenced by a narrow band of high surface-ocean chlorophyll values (Wang et al., 2005), in an otherwise oligotrophic pelagic setting (Figure 1).

1.4. Oceanography of the Oligo-Miocene Eastern Equatorial Pacific Ocean

On geological time scales, the sustained equatorial upwelling of nutrient rich waters has resulted in a regionally more efficient BCP (i.e., net transport of particulate organic carbon to the deep sea), carbon sequestration in the deep waters, and ultimately in relatively high rates of export productivity, as is evidenced by a substantial equatorial sediment bulge (Lyle et al., 2008; Mitchell et al., 2003). The amount of exported biogenic carbonate, augmented by a varying biogenic silicate contribution, deposited beneath the equatorial upwelling zone is so substantial, that the bulge is elevated by ∼600 m relative to the surrounding abyssal plane (Mitchell et al., 2003).

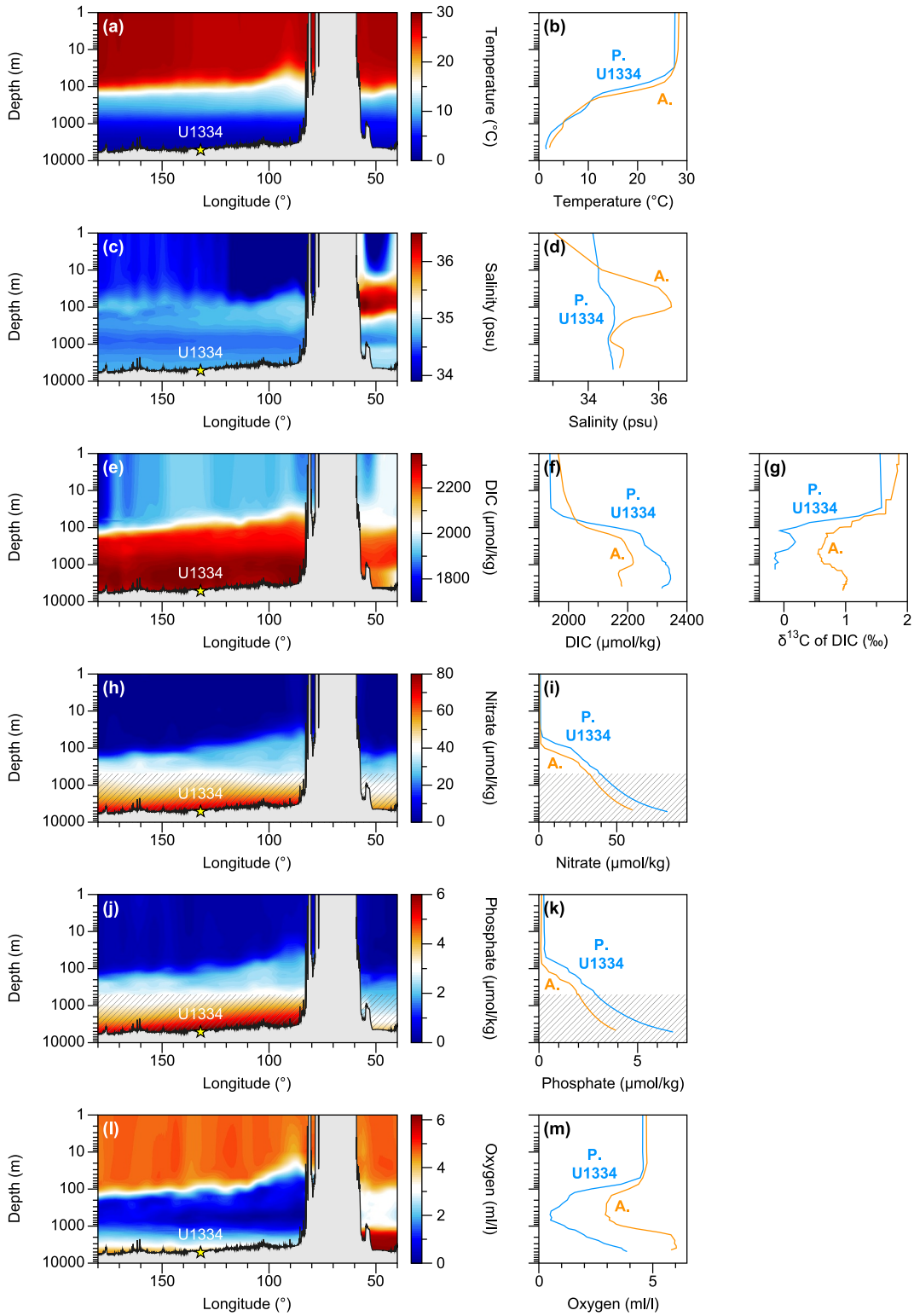

Figure 2. Present-day water column oceanographic context of the EEP. Please note that depth is plotted on a logarithmic scale. Panels (a–m) As in Figure 1, except for panel (g) which depicts the (estimated) $\delta^{13}C$ of DIC. Hashed areas indicate extrapolated values. "P U1334" stands for Pacific Ocean Site U1334 at 8° latitude and 132° longitude. "A" stands for Atlantic Ocean at 8° latitude and 50° longitude.

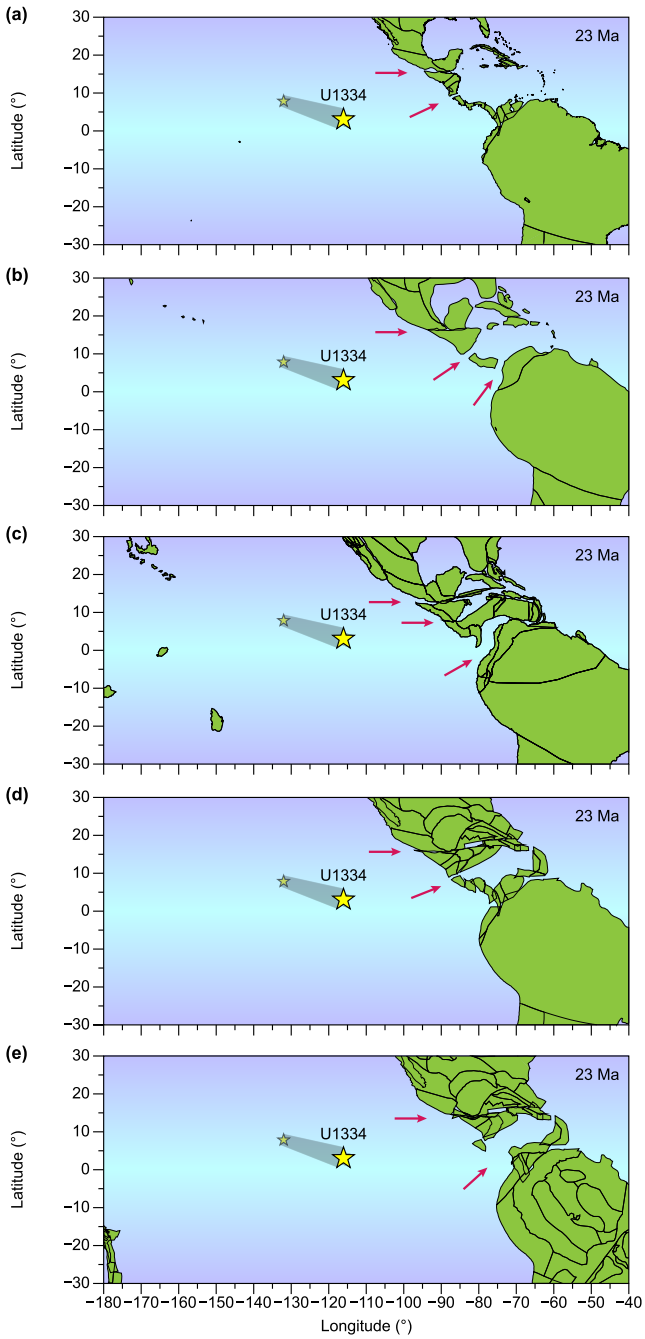

Figure 3. Oligo-Miocene geographic context of the EEP. Continental plate polygons for 23 Ma using reconstructions of (a) Cao et al. (2017), (b) "Scotese paleomap," (c) Hay et al. (1999), (d) "Global EarthByte," and (e) Merdith et al. (2021). Panels (a), (b), (d), and (e) were generated in GPlates (Müller et al., 2018). Panel (c) was generated using https://www.odsn.de. Please note, these reconstructions are not presented as testable hypotheses, but to depict the uncertainty and variability among available CAS reconstructions at 23 Ma. These plate polygons may shed light on where (a) deep-water connection(s) between the Atlantic and Pacific Oceans may have been situated (see arrows). However, potential localities for shallow-water connections cannot be derived from these plate polygon reconstructions only and may have been more geographically extensive than these reconstructions suggest.

This flux of carbon, from the exogenic to the endogenic carbon reservoir, is key in modulating Earth's thermostat on these longer time scales. The varying strength of the biological pump on astronomical (e.g., eccentricity) time scales in the EEP through time is an important, but poorly constrained process in investigations into past global carbon cycling (Bolton et al., 2011; Ford et al., 2012; Lyle et al., 2008; Ma et al., 2015).

The CAS (Figure 3), together with the Tethys Ocean (i.e., an equatorial connection between the Indian and Atlantic Oceans) and a more open Indonesian Gateway (Gallagher et al., 2024), facilitated globe encompassing trans-equatorial circulation up to at least the OMT (Kennett et al., 1985). As a result, oceanic circulation patterns in the EEP would have differed substantially (Fraass et al., 2019; von der Heydt & Dijkstra, 2005, 2006). ENSO variability across in the Miocene is thought to have been more intense, yet less frequent (von der Heydt & Dijkstra, 2006). Irrespective of the presence/absence of a CAS, there was likely a proto-cold tongue in the EEP from the mid-Eocene onward resulting from largely stable trade winds and the equatorial divergence (Lyle et al., 2002; Moore Jr. et al., 2004; Wade et al., 2020). However, the presence of the CAS would have permitted the equatorial transport of heat, salinity, nutrients, and oxygen (von der Heydt & Dijkstra, 2005, 2006), as well as biota (Fraass et al., 2019), between the Atlantic and Pacific Oceans. Direction of flow through the CAS is thought to have changed from a west-ward (from Atlantic to Pacific) to an east-ward (from Pacific to Atlantic) flow direction across the OMT on at least one occasion (Fraass et al., 2019; von der Heydt & Dijkstra, 2005), as is documented by the delayed appearance in the Atlantic Ocean (perhaps by up to 300 Kyr) of the Indo-Pacific-originating, (sub-)tropical, planktonic foraminifer *Paragloborotalia kugleri* (Fraass et al., 2019). Corroborating evidence for changing surface ocean conditions surrounding the CAS is a regional, Caribbean coral extinction and restriction event, potentially linked to (a) glacioeustatic sea level lowstand(s), change in surface ocean temperatures and/or nutrient availability (Edinger & Risk, 1994). We note, however, that the exact paleogeography of the CAS is highly uncertain (Figure 3) due to poor constraints on the drift of plate polygons in the vicinity of the CAS (Cao et al., 2017; Hay et al., 1999; Merdith et al., 2021; Müller et al., 2018). One or several deep-water connections between the Atlantic and Pacific Oceans may have been present (Figure 3). However, detailed information about the geographic extent of surface ocean connectivity is beyond available reconstructions (Montes et al., 2012).

2. Materials and Methods

2.1. Site Description

IODP Site U1334 (7°59′N, 131°58′W), was drilled during Expedition 320 at a water depth of 4.8 km, and it is estimated to have had a paleo-water depth of ∼4.1 km during the late Oligocene and early Miocene (Pälike et al., 2010). During this time the carbonate compensation depth was situated at ∼4.7 km water depth, allowing for the preservation of biogenic carbonate rich sediments at Site U1334 (Pälike et al., 2012). The site is positioned on ∼38 Ma old crust, targeted the EOT, yet also recovered a continuous Oligocene and OMT-spanning sedimentary sequence. Furthermore, the site is particularly suitable for investigations into the OMT, because at this time, at around 23 Ma, it was situated almost exactly at the equator (around 3°N and −116°W, Figures 1 and 3) and within the equatorial upwelling zone, resulting into a relatively

expanded late Eocene to early Miocene section (Pälike et al., 2010). Previous investigations have shown that these sediments constitute a valuable archive of biogenic carbonates and silicates, that can be used to reconstruct past climate and carbon cycle conditions, such as astronomically forced changes in deep-sea temperatures and/or ice volume, paleo-productivity, and the carbonate compensation depth (Beddow et al., 2016, 2018; Lyle et al., 2008; Pälike et al., 2012).

2.2. Sample Processing and Taxonomic Concepts

For this study (Beddow, 2016), four species of planktonic foraminifera were picked (where present) for stable isotope analysis from the same samples previously used to generate benthic foraminiferal isotope records (Beddow et al., 2016, 2018). These planktonic foraminifera are the mixed-layer photosymbiotic species *Trilobatus primordius* (until recently *Globigerinoides primordius* (Spezzaferri et al., 2015)) and *Globigerinoides altiaperturus*, and the thermocline dwelling asymbiotic species *Paragloborotalia siakensis* (Figure 4) and *Dentoglobigerina venezuelana* (Figure 5). We note that *D. venezuelana* is highly variable in morphology (Wade et al., 2018), and restricted picking to specimens with a circular outline and 3½ to 4 embracing, reniform chambers that gradually increase in size (Figure 5). To mitigate isotopic variability resulting from (seasonal) life-cycle changes in calcification depth, we preferentially picked adult individuals in the 250–355 μm size fraction.

2.3. Scanning Electron Microscope Analysis

To assess the preservation and morphological variability of the most-abundant planktonic foraminifera, 14 representative specimens of *P. siakensis* (Figure 4) and *D. venezuelana* (Figure 5) were picked for scanning electron microscope (SEM) analysis. These specimens were mounted in umbilical view on a SEM stub and coated in gold using a sputter coater. The samples were imaged using a JEOL JSM-6480LV variable pressure SEM at University College London. All specimens were imaged with a view of the whole test to ensure both species were consistent with the taxonomic descriptions (Leckie et al., 2018; Wade et al., 2018). In addition, the test wall of selected specimens was imaged at a high magnification (>1,000x) to analyze the preservation state of the sample.

2.4. Stable Isotope Mass Spectrometry

Prior to stable isotope analysis, we combine multiple (i.e., between two and six) individual tests, depending on abundance, to average the effect of seasonal and/or depth differences at the time of calcification (Pearson, 2012). Tests were suspended in ethanol and ultrasonically cleaned. Subsequently, the samples were dried at 40°C and crushed prior to mass-spectrometry. Stable oxygen ($\delta^{18}O$) and carbon ($\delta^{13}C$) isotope analyses were conducted at Utrecht University, using a Thermo-Finnigan Kiel III automated preparation system coupled to a Thermo-Finnigan MAT 253 isotope ratio mass-spectrometer. The standards NBS-19 and "Naxos" (in-house) were used to calibrate isotope values to the Vienna Pee Dee Belemnite. Analytical precision was 0.08 and 0.03‰ for $\delta^{18}O$ and $\delta^{13}C$, respectively. Twelve outlying values were defined by eye (i.e., highly aberrant single values that were not in line with overall trends, signals, and/or amplitude variability ranges) from the *D. venezuelana* $\delta^{18}O$ and $\delta^{13}C$ data set and remeasured where possible. We compare the planktonic $\delta^{18}O$ and $\delta^{13}C$ records to published benthic $\delta^{18}O$ and $\delta^{13}C$ data set measured on the species *Cibicidoides mundulus* and *Oridorsalis umbonatus* (Beddow et al., 2016, 2018). These benthic foraminiferal stable isotope data were generated on the same samples and in the same laboratory.

2.5. Depth and Age Models

For this study, we used the latest splice (Westerhold, Röhl, Wilkens, et al., 2012) and $CaCO_3$ tuned age model (Beddow et al., 2018), which was calibrated to the La2011 eccentricity solution (Westerhold, Röhl, & Laskar, 2012). In a broader effort to integrate drill sites from the EEP into a single Cenozoic stratigraphy (Westerhold et al., 2020), we transferred Site U1334 depth to Site 1218 depth prior to reassigning the eccentricity tuning tie points of the $CaCO_3$ tuning in Beddow et al. (2018). This yielded negligible differences (±5 Kyr) compared to the original age model, mainly resulting from small uncertainties in the precise depth correlation between Sites 1218 and U1334. In addition, we corrected for a small discrepancy of ~25 Kyr between $CaCO_3$ tuned ages and those based on plate-pair spreading rates (Beddow et al., 2018), by relaxing (i.e., deleting) a tuning tie point at the eccentricity minimum at 22.954 Ma. This adjustment brings the original $CaCO_3$ tuning in even closer agreement with plate-pair spreading models and removes the artificial "stretching" of Chron C6Cn.1r at the expense of the

10.1029/2024PA004892

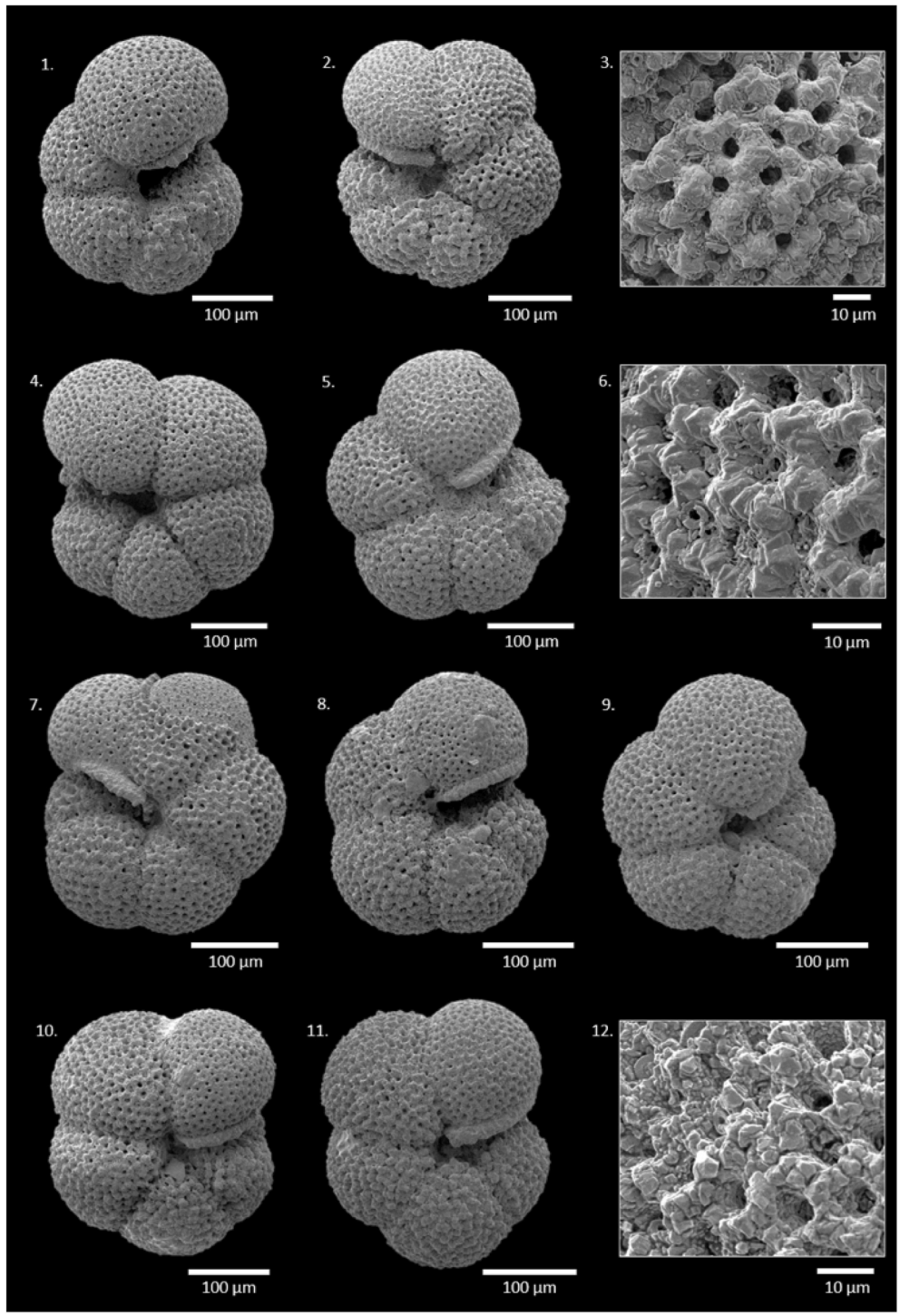

Figure 4. Scanning electron micrographs of planktonic foraminifera *Paragloborotalia siakensis* from Hole U1334A. **(1)** 11H-4, 110–111 cm, 112.23 m CCSF-A. **(2–3)** 11H-5, 28–29 cm, 112.91 m CCSF-A. **(4)** 11H-5, 68–69 cm, 113.31 m CCSF-A. **(5–7)** 11H-5, 100–101 cm, 113.63 m CCSF-A. **(8–9)** 11H-5, 108–109 cm, 113.71 m CCSF-A. **(10–12)** 11H-5, 116–117 cm, 113.79 m CCSF-A.

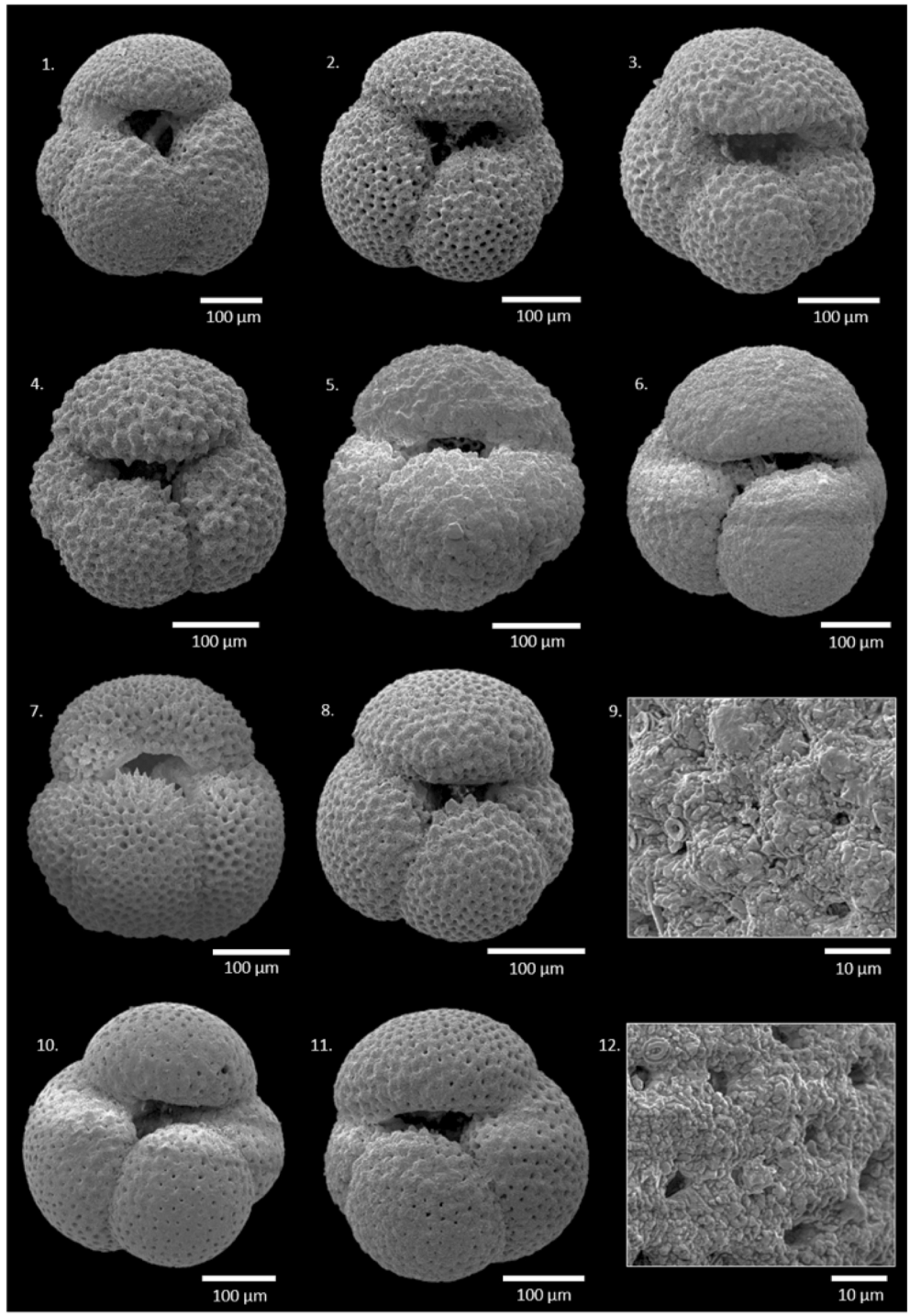

Figure 5. Scanning electron micrographs of planktonic foraminifera *Dentoglobigerina venezuelana* from Hole U1334A. **(1)** 11H-4, 46–47 cm, 111.59 m CCSF-A. **(2)** 11H-4, 110–111 cm, 112.23 m CCSF-A. **(3)** 11H-5, 28–29 cm, 112.91 m CCSF-A. **(4–5)** 11H-5, 68–69 cm, 113.31 m CCSF-A. **(6)** 11H-5, 96–97 cm, 113.59 m CCSF-A. **(7)** 11H-5, 100–101 cm, 113.63 m CCSF-A. **(8–9)** 11H-5, 108–109 cm, 113.71 m CCSF-A. **(10–12)** 11H-5, 116–117 cm, 113.79 m CCSF-A.

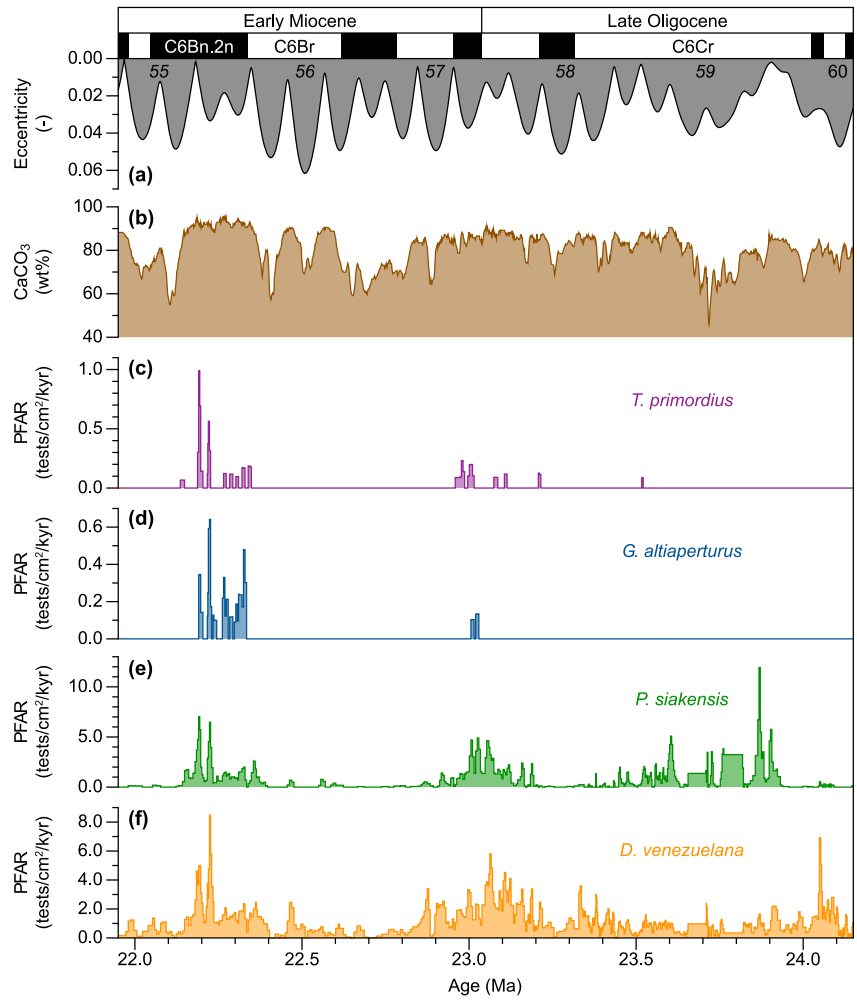

Figure 6. Planktonic foraminiferal accumulation rates. (a) Magnetostratigraphy of Site U1334 and the La2011 eccentricity solution. The 405-Kyr eccentricity Cycle Numbers are indicated. The position of the Oligocene-Miocene boundary corresponds to the base of Chron C6Cn.2n. (b) Estimated $CaCO_3$ content based on a calibration of magnetic susceptibility to coulometric measurements of carbonate content. (c–f) Species specific PFARs.

"squeezing" of Chron C6Cn.2n in the original $CaCO_3$ tuned age model (Beddow et al., 2018). To calculate species-specific planktonic foraminifer accumulation rates (PFARs) we multiplied the total number of planktonic foraminiferal tests (i.e., in the 250–355 μm size fraction) per gram by mass accumulated rates (MARs) (Figure 6) (Diester-Haass et al., 2011). In turn, MARs were computed by multiplying linear sedimentation rates (this study, based on Beddow et al. (2018)) by the dry bulk density (Pälike et al., 2010). It is important to realize that PFARs, like all change rates, depend on the age model, which in the case of Site U1334 is based on astronomical tuning to Earth's eccentricity solution (Figure 6). However, the overall structure and long-term cyclicity of the PFAR records is a robust feature that can readily be observed in the records of the total number of planktonic foraminiferal tests in the stratigraphic depth domain.

3. Results

3.1. Planktonic Foraminiferal Morphology and Preservation

Specimens of *T. primordius* and *G. altiaperturus* are taxonomically consistent with previous studies (Spezzaferri et al., 2018). For *P. siakensis* (Figure 4), most specimens have 5–6 chambers in the final whorl, moderately depressed radial sutures, and an umbilical to extra-umbilical aperture bordered by a distinctive lip. While some specimens have more enveloping and kummerform (i.e., small and stunted) final chambers (e.g., specimens 2, 10,

and 11, Figure 4), the imaged specimens are consistent with specimens from the type locality presented in Zachariasse and Sudijono (2012). The specimens of *D. venezuelana* (Figure 5) are relatively consistent in terms of morphology, with only a small degree of variance in their morphological characteristics. Visually, foraminifera from the Oligocene-Miocene interval of Site U1334 appear moderately preserved, with the preservation being poorer compared to the early to middle Miocene of Site U1338 (Fox & Wade, 2013; Fox et al., 2021). In general, infilling is rare, but foraminifera are partially dissolved and/or recrystallized. The most common post burial alteration is the presence of coccoliths on the foraminiferal test wall. The degree of recrystallization appears to increase downcore, especially in the older, Oligocene samples (i.e., Figures 4(12) and 5(12)).

3.2. Planktonic Foraminiferal Accumulation Rates

On the eccentricity tuned age model, our data cover the late Oligocene and early Miocene epochs, between ~24.15 and 21.95 Ma, including the OMT at around 23.0 Ma. The records span 405-Kyr Eccentricity Cycles 60 to 55 (Figure 6), counted from 405 Kyr eccentricity minimum to 405 Kyr eccentricity minimum, broadly corresponding to an earlier eccentricity cycle numbering scheme that counts from mid-cycle to mid-cycle (Pälike, Norris, et al., 2006; Wade & Palike, 2004; Wade et al., 2011). Our 405-Kyr eccentricity based astrochronozones are concurrent with magnetochrons C6B and C6C (Hilgen et al., 2020; Liebrand et al., 2016). PFAR are highly variable and species dependent (Figure 6). Overall, the most abundant and nearly continuously present planktonic foraminifer species is *D. venezuelana* with PFARs ranging between 0 and 9 tests/cm^2/Kyr. The next most abundant planktonic foraminifer species is *P. siakensis*, which PFAR are marked by values ranging from 0 to an absolute maximum of 12 tests/cm^2/Kyr at ~23.9 Ma. We note, however, that the *P. siakensis* record is not as continuous as that of *D. venezuelana*. Both the *D. venezuelana* and the *P. siakensis* PFARs show a modest 405-Kyr pacing, with maximum PFARs during 405-Kyr eccentricity minima (Figure 6). In contrast to this relatively continuous presence of thermocline-dwelling planktonic foraminiferal tests in the sediments, mixed-layer dwellers *Globigerinoides* and *Trilobatus* are only present intermittently throughout the study interval. Both the *G. altiaperturus* and the *T. primordius* PFARs range between 0 and 1 tests/cm^2/Kyr from 22.4 until 22.1 Ma, concurrent with the 405 Kyr eccentricity minimum "between" Cycles 56 and 55. They are almost completely absent for the rest of the study interval, during both eccentricity maxima and minima (Figure 6).

3.3. Foraminiferal $\delta^{18}O$ and $\delta^{13}C$ Records

Some key observations from the combined planktonic and benthic foraminiferal $\delta^{18}O$ records (Figures 7 and 8) are that (a) the maximum $\delta^{18}O$ values of 2.9‰, reached by *O. umbonatus*, concur with the peak of the OMT glaciation/global cooling, (b) the increase in $\delta^{18}O$ values during peak OMT conditions, so strongly expressed in both previously published benthic foraminiferal $\delta^{18}O$ records (Beddow et al., 2016, 2018), is much delayed, of smaller amplitude, and altogether differently structured in the *D. venezuelana* $\delta^{18}O$ record, and (c) the *D. venezuelana* $\delta^{18}O$ record is marked by a substantial increase in amplitude variability during the early Miocene, compared to the late Oligocene. Some key observations from the combined planktonic and benthic foraminiferal $\delta^{13}C$ records (Figures 7 and 9) are that (a) the CM-OM positive isotope excursion is present in all foraminiferal $\delta^{13}C$ records (b) the carbon isotopic fractionation between bottom waters (as recorded in *C. mundulus* $\delta^{13}C$) and pore waters (as recorded in *O. umbonatus* $\delta^{13}C$) is much more pronounced compared to isotopic fractionation within the water column (i.e., between planktonic and epifaunal benthic foraminiferal $\delta^{13}C$), (c) the increase in higher frequency amplitude variability during the early Miocene in the *D. venezuelana* $\delta^{18}O$ record is absent from the *D. venezuelana* $\delta^{13}C$ record, and (d) the difference, or vertical gradient, between *D. venezuelana* and *C. mundulus* $\delta^{13}C$ records increases with time and is generally most amplified during 405 Kyr eccentricity cycle minima.

3.4. Amplitude Variability of Foraminiferal $\delta^{18}O$ and $\delta^{13}C$

To distill more features from the somewhat noisier "raw" species-specific isotope records (Figures 8 and 9), we compute smooths (Marron & Zhang, 2005), including ±1 standard deviation (SD) variability estimates, and linear trends across the study interval, on the three highest resolution $\delta^{18}O$ and $\delta^{13}C$ records of *D. venezuelana*, *C. mundulus*, and *O. umbonatus* (Figure 10). We consider the isotope records of *P. siakensis*, *G. altiaperturus*, and *T. primordius* too poorly resolved (Figures 8 and 9) for smoothing and trending. The smooths and linear trend lines visualize both the long-periodic orbital variability (i.e., 405 Kyr eccentricity and longer) and secular change over

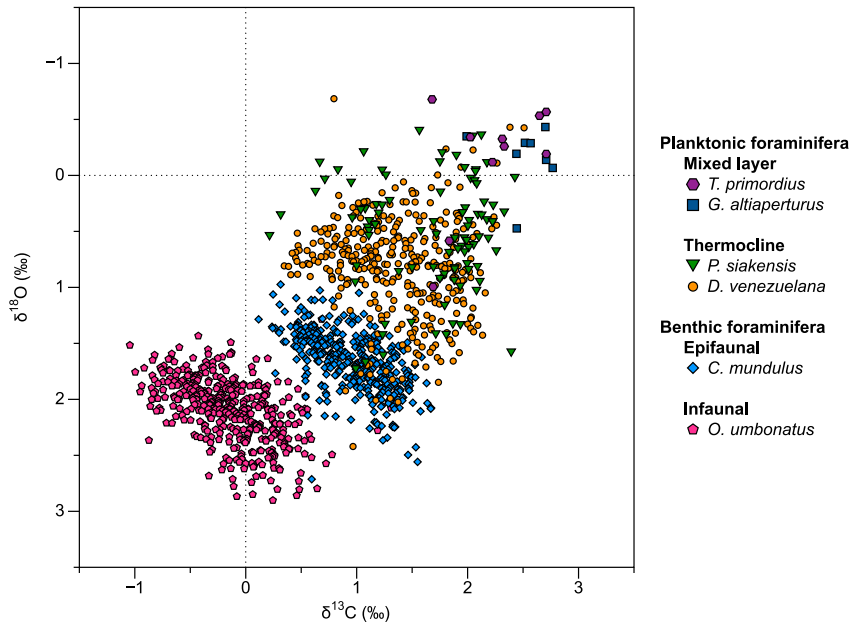

Figure 7. Foraminiferal water column/sediment depth-habitats. The grouping of isotopic values in clusters for each species indicates that despite visual evidence for modest dissolution and/or recrystallization (see Figures 4 and 5) a primary isotopic depth-habitat signal is preserved in Oligo-Miocene foraminifera from Site U1334.

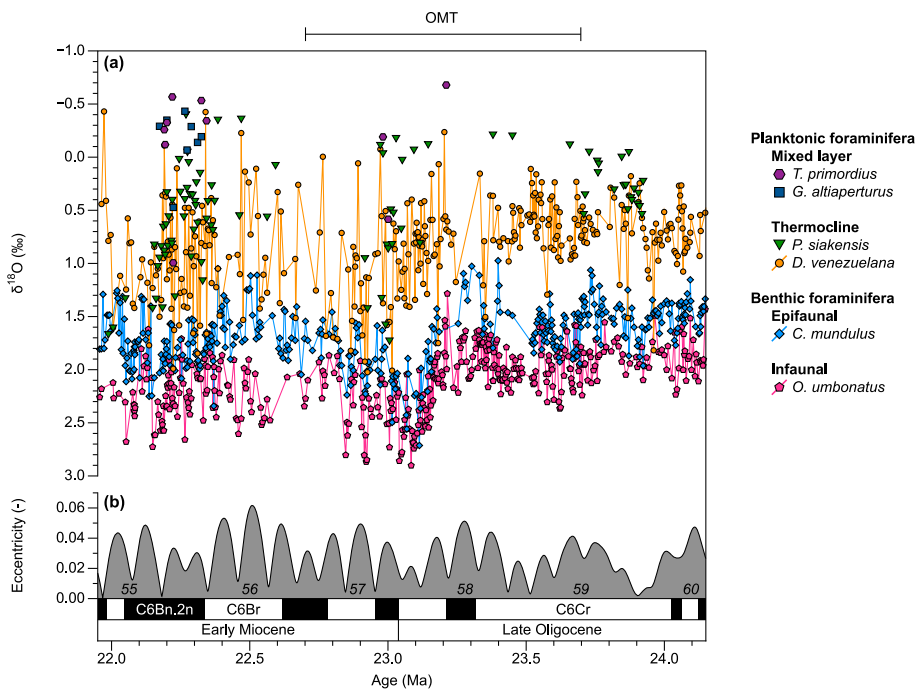

Figure 8. Foraminiferal $\delta^{18}O$ records across the Oligo-Miocene Transition (OMT). (a) Planktonic and benthic foraminiferal $\delta^{18}O$ records from Site U1334 on the eccentricity tuned age model. (b) Magnetostratigraphy of Site U1334 and the La2011 eccentricity solution. The 405-Kyr eccentricity Cycle Numbers are indicated.

10.1029/2024PA004892

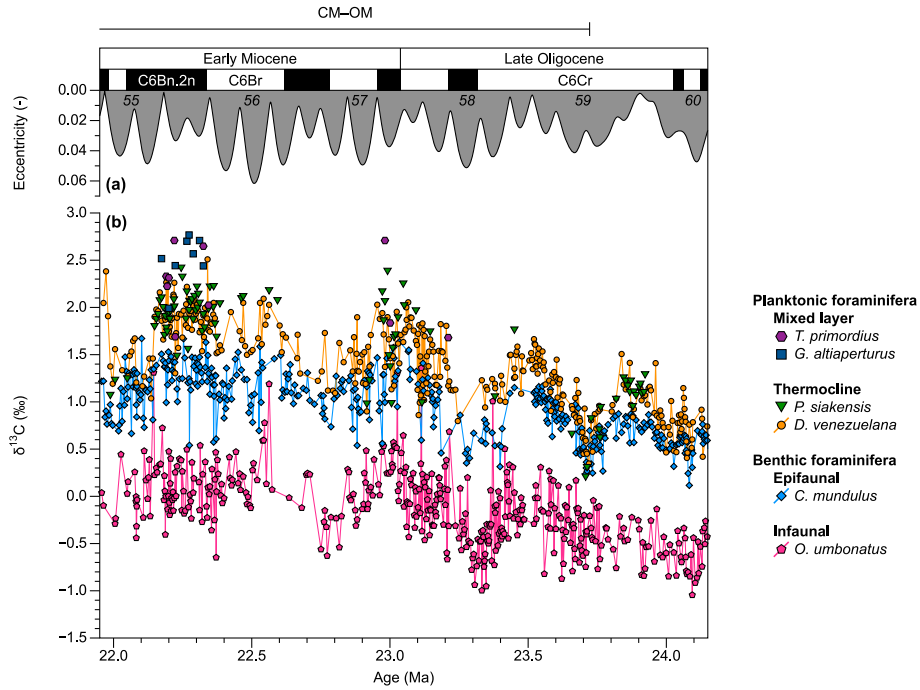

Figure 9. Foraminiferal $\delta^{13}C$ records across the Oligo-Miocene Transition. (a) Magnetostratigraphy of Site U1334 and the La2011 eccentricity solution. The 405-Kyr eccentricity Cycle Numbers are indicated. (b) Planktonic and benthic foraminiferal $\delta^{13}C$ records from Site U1334 on the eccentricity tuned age model. CM-OM stands for Oligocene-Miocene carbon maximum.

the study interval, respectively. Due to the uneven data resolution of these individual records, we refrain from computing subsurface-to-deep ocean vertical isotope gradients. However, we do display them as shaded areas to aid the discussion (Figure 11). Furthermore, we caution against statistical (over) interpretations of the short-term variability (i.e., ~110 Kyr eccentricity and shorter) within and between the records, such as frequency coherences and phase relationships. For longer periodic signals (i.e., 405 Kyr eccentricity and longer) such statistical processing is also not recommended, due to the relatively short time span of our records, and hence, the low number of long-periodic cycles present.

Linear trend lines in $\delta^{18}O$ are marked by broadly similar positive slopes among the *D. venezuelana*, *C. mundulus*, and *O. umbonatus* records, even though the slope of the *C. mundulus* $\delta^{18}O$ trend line is slightly less steep than the other two (Figure 10a). Most remarkable, and better visualized in the smoothed records, is the heterogeneous expression of the (transient) $\delta^{18}O$ increase across the OMT at ~23.0 Ma. A stepwise increase is observed in the infaunal benthic foraminiferal $\delta^{18}O$ record of *O. umbonatus*, with $\delta^{18}O$ values varying around ~1.9‰ between 24.1 and 23.2 Ma, and around ~2.3‰ between 23.2 and 22.0. The excursion itself is up to ~1.1‰ within the ±1 SD variability estimates (Figure 10). A more transient increase across the OMT is present in the epifaunal benthic foraminiferal $\delta^{18}O$ record of *C. mundulus*. The excursion in this record is marked by a maximum $\delta^{18}O$ increase of ~1.5‰ within the ±1 SD variability estimates. In the smooth of the *D. venezuelana* $\delta^{18}O$ record, the much delayed (relative to the benthic records) and largely transient increase in $\delta^{18}O$ becomes more apparent. Its maximum amplitude is 1.7‰ within the ±1 SD variability estimates. Furthermore, the large increase in the range of variability in the *D. venezuelana* $\delta^{18}O$ record can now also be better constrained. The late Oligocene interval is marked by a range of ~0.5‰ around the mean, whereas the early Miocene interval is characterized by a range of ~1.0‰ around the mean (Figure 10).

Like the linear trend lines in the $\delta^{18}O$ values, those computed on the species' $\delta^{13}C$ values have comparable positive slopes across the study interval (Figure 10b). However, the *C. mundulus* $\delta^{13}C$ trend line, like the *C. mundulus* $\delta^{18}O$ trend line, is less pronounced. The smoothed foraminiferal $\delta^{13}C$ records show in greater clarity on long-periodic orbital time scales and is most strongly expressed in the *D. venezuelana* $\delta^{13}C$ record, with nearly every 405 Kyr eccentricity maximum (minimum) corresponding to a $\delta^{13}C$ minimum (maximum). The one

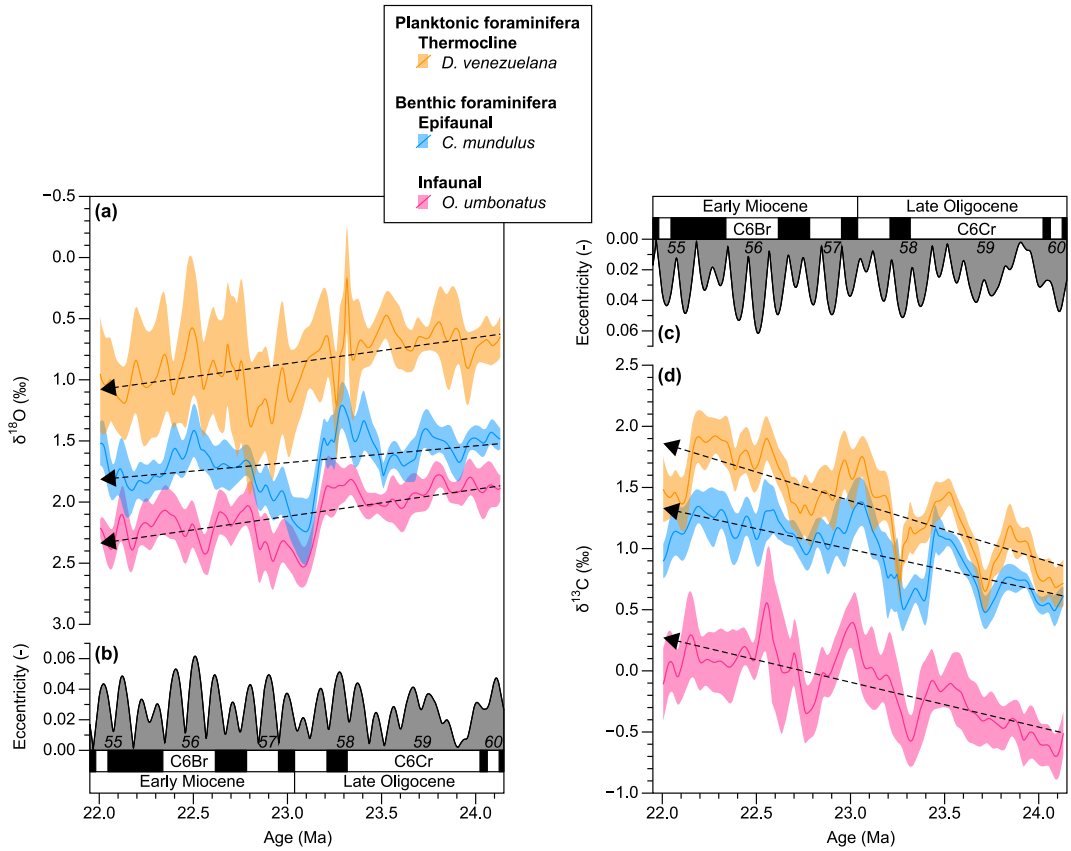

Figure 10. Smoothed foraminiferal $\delta^{18}O$ and $\delta^{13}C$ records from Site U1334. (a) Smoothed planktonic (*D. venezuelana* only) and benthic foraminiferal $\delta^{18}O$ records ±1 standard deviation (shaded areas). (b, c) Magnetostratigraphy of Site U1334 and the La2011 eccentricity solution. The 405-Kyr eccentricity Cycle Numbers are indicated. (d) Smoothed planktonic (*D. venezuelana* only) and benthic foraminiferal $\delta^{13}C$ records ±1 standard deviation (shaded areas).

exception in 405 Kyr response occurs at 22.7 Ma, directly post-OMT and concurrent with the main body of the CM-OM, when a pronounced $\delta^{13}C$ minimum occurs during a 405 Kyr eccentricity minimum. During three 405 Kyr eccentricity maxima, at ~23.7, ~23.2, and ~22.1 Ma, the *D. venezuelana* $\delta^{13}C$ approach *C. mundulus* $\delta^{13}C$ values, reducing (i.e., "collapsing") the between-species isotope gradients to an absolute minimum (Figure 11). Variability in smoothed *O. umbonatus* $\delta^{13}C$ is of very high amplitude and is potentially affected by a few high values/remaining outliers and gaps in record, making it more difficult to untangle the (potential) response to the 405 Kyr eccentricity cycle.

4. Discussion

4.1. Diagenetic and Ontogenetic Effects on Foraminiferal Isotope Values

Before we can interpret our foraminifer $\delta^{18}O$ and $\delta^{13}C$ records in terms of climate, land-ice, ocean, and carbon cycle variability through time, we need to briefly address isotopic overprints and other effects on absolute isotopic values, for example, due to calcification out of equilibrium with sea-water, caused by: (a) recrystallization (Pearson et al., 2001; Sexton et al., 2006), (b) changes in depth habitat and ecology due to vertical water column migrations on seasonal, ontogenetic (i.e., life cycle), or evolutionary time scales, and/or (c) evolutionary adaptations in which photosymbionts are acquired or lost between 24.15 and 21.95 Ma. Of these potential "biases" on isotopic ratios, bias (a) can affect both planktonic and benthic foraminiferal isotope values, whereas biases (b) and (c) can only affect the planktonic foraminiferal isotope values considered here. The grouping of isotopic values into distinct clusters for each species in the $\delta^{18}O$-$\delta^{13}C$ space (Figure 7) indicates that, despite moderate recrystallization (Figures 4 and 5), a primary isotopic signal is still preserved. We infer that these primary signals

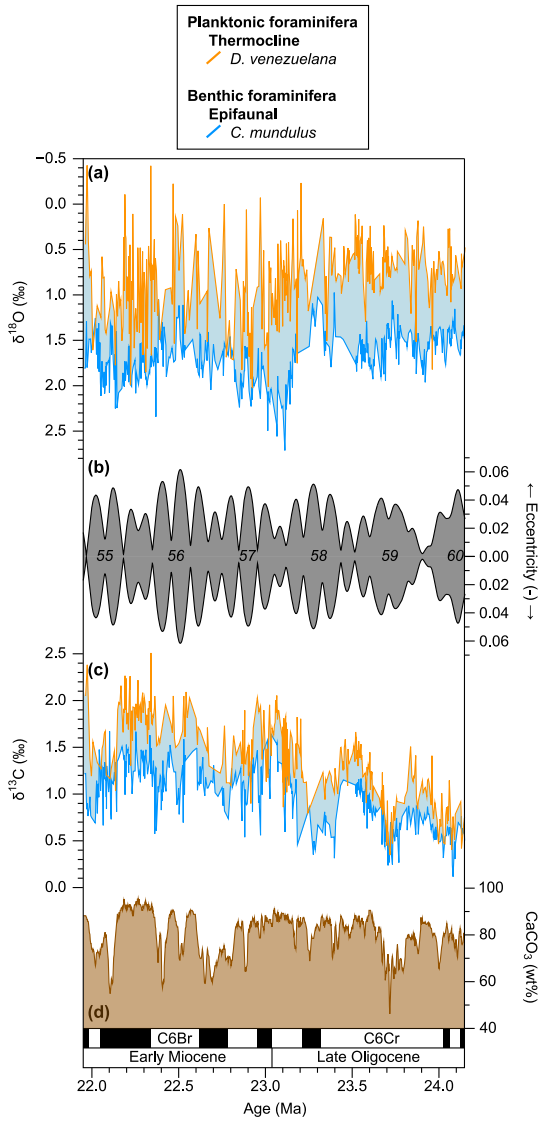

Figure 11. Climate, carbon cycle, and productivity variability as recorded at Site U1334. (a) The *D. venezuelana* versus the *C. mundulus* $\delta^{18}O$ record. (b) The La2011 eccentricity solution. Note that eccentricity is depicted two times to match the different (dominant) 405 Kyr responses of both $\delta^{18}O$ and $\delta^{13}C$, whilst keeping the proxy records ordered by water column/calcification depth. (c) The *D. venezuelana* versus the *C. mundulus* $\delta^{13}C$ record. (d) Estimated $CaCO_3$ content based on a calibration of magnetic susceptibility to coulometric measurements of carbonate content. Below, the magnetostratigraphy of Site U1334.

reflect a combination of habitat during ontogeny/calcification depth in the water column, or inside the sediment in case of infaunal *O. umbonatus*, and the presence or absence of photosymbionts, in case of the planktonic species, because the time-averaged species-specific isotopic fingerprints (Figure 7), remain largely stable throughout the study interval (Figures 8–10). This observation also holds true for the OMT and no relative inversions between species in either $\delta^{18}O$ or $\delta^{13}C$ isotope space are observed. We can thus conclude that no major changes in (average) depth habitat or photosymbiont acquisition/loss occurred in the EEP during the 24 to 22 Ma Oligo-Miocene time-interval considered here.

4.2. Planktonic Foraminiferal Depth Habitat During the Oligo-Miocene

Both *T. primordius* and *G. altiaperturus* record the most negative $\delta^{18}O$ and most positive $\delta^{13}C$ values (Figure 7) consistent with a mixed layer photosymbiotic life cycle (Spezzaferri et al., 2018). The relative positioning of both the *P. siakensis* and *D. venezuelana* specimens from Site U1334 in $\delta^{18}O$-$\delta^{13}C$ space with respect to the other planktonic and benthic foraminifer species, supports that they were asymbiotic upper (Leckie et al., 2018; Pearson & Wade, 2009) and lower (Beasley et al., 2021; Gasperi & Kennett, 1993; Pearson & Wade, 2009; Pearson et al., 1997; Wade et al., 2007) thermocline dwelling species, respectively, during the Oligo-Miocene interval covered in this study (Figure 7). At Site U1334 the thermocline corresponds to the boundary between EUC/EqPIW and PDW (Rippert et al., 2017), from which we infer that these species probably lived between ~100 and 200 m water depth (Figures 2a and 2b), and below the deep chlorophyll maximum at around 50–100 m water depth (Cornec et al., 2021). For *D. venezuelana*, this inferred Oligocene-Miocene depth habitat contrasts with those inferred for earlier and later Oligo-Miocene time intervals. Considering all evidence, *D. venezuelana* changed its depth-habitat more permanently, on evolutionary time scales, from a relatively shallow position in the mixed layer (i.e., a shallow thermocline habitat) during the early (Moore et al., 2014) and "mid" Oligocene (Wade & Palike, 2004), to a deeper position in the thermocline during the late Oligocene ((Matsui et al., 2016; Stewart et al., 2012; Wade & Palike, 2004), this study). In addition to these (apparent) long-term adaptive/evolutionary trends in depth habitat of *D. venezuelana* in the EEP, isotope values of *D. venezuelana* change through ontogeny with larger specimen living deeper in the water column (Stewart et al., 2012; Wade et al., 2007). However, we can largely rule out these ontogenetic effects on our record, as multiple specimens from a restricted size fraction (250–355 μm) were analyzed. Another potential effect on *D. venezuelana* isotope values are vertical migrations/habitat changes on astronomical time scales, for example, the 405 Kyr time scales under consideration here. The ~405 Kyr signal in *D. venezuelana* PFARs may provide tentative evidence for this hypothesis. However, further work is needed to better constrain potential migrations on eccentricity (and shorter astronomical) time scales.

4.3. Cryospheric, Climatic, and Oceanographic Controls on Foraminiferal $\delta^{18}O$

Species-specific and habitat fractionation can explain the different incorporation of $\delta^{18}O$ into the calcite of different species of foraminifera, thereby explaining their consistent offsets in absolute values (Pearson, 2012; Rohling & Cooke, 1999). However, long term trends and orbital variability captured in foraminiferal $\delta^{18}O$ values of a particular species, are a function of ambient temperature and salinity, and global land-ice volumes, with lower (higher) temperature, higher (lower) salinities, and higher (lower) land-ice volumes contributing to higher (lower) foraminiferal $\delta^{18}O$ values. The exact (species specific) partitioning of the integrated $\delta^{18}O$ signal among these

three parameters can only be quantified with additional independent temperature, land-ice volume, and/or salinity proxy data (Meckler et al., 2022), which are currently unavailable for Oligo-Miocene interval from Site U1334. However, despite these limitations, we can explore, albeit somewhat more speculatively, which processes were more likely to have governed the various species-specific $\delta^{18}O$ records, by comparing when signals are homogeneous between planktonic, and epifaunal and infaunal benthic $\delta^{18}O$ records, suggesting (a) common cause(s), and when patterns in the records are more heterogeneous, suggesting several independent causes.

On time scales longer than the mixing time of the oceans (i.e., ~1 Kyr), the land-ice volume effects on $\delta^{18}O$ values of both planktonic and benthic foraminifera is presumed to be of similar amplitude. Therefore, we interpret the positive trends, marked by largely comparable slopes, to reflect the increase in land-ice volume on Antarctica across the OMT (Figure 10). Similarly, part of the variability that is shared between planktonic and benthic foraminiferal $\delta^{18}O$ records on shorter, orbital time scales can also be attributed to Antarctic land-ice volume variability (Figures 8 and 10). However, due to the more variable, or noisier character of the *D. venezuelana* $\delta^{18}O$ record, quantifying what part of the planktonic and benthic $\delta^{18}O$ records is shared on orbital time scales is dependent on arbitrary choices of time series analysis (e.g., filter width). We attribute residual signals in the *D. venezuelana*, *C. mundulus*, and *O. umbonatus* $\delta^{18}O$ records, that is, where they are no longer in close agreement among each other (Figures 8 and 10), to more ambient temperature and salinity effects on $\delta^{18}O$. For example, the greater amplitude of the transient OMT glaciation in the *C. mundulus* $\delta^{18}O$ record compared to the *D. venezuelana* $\delta^{18}O$ record, probably reflects the enhanced cooling of the higher latitudes, where AABW and PDW formed, compared to tropical surface waters in which *D. venezuelana* and other planktonic foraminifera built their tests. Alternatively, greater variability in (astronomically forced) latitudinal ITCZ migrations may have affected surface ocean temperatures considerably, thereby explaining the enhanced early Miocene *D. venezuelana* $\delta^{18}O$ variability. Such a hypothesis is supported by a documented increase in Asian dust deposited in the EEP and the associated southward migration of the ITCZ during the OMT (Hyeong et al., 2014). Lastly, a (temporary) flow reversal through the CAS, from westward to eastward (Fraass et al., 2019), may have reduced the amount of more saline Atlantic surface/intermediate waters (Figures 1b, 2c, and 2d) from entering the surface/intermediate EEP, thereby attenuating the OMT (temperature) signal in the *D. venezuelana* $\delta^{18}O$ record. However, planktonic foraminiferal $\delta^{18}O$ records suggest that large isotopic gradients did not evolve until the Pliocene (~4.2 Ma), when the CAS became effectively restricted (Haug et al., 2001), and the EEPs modern-like cold tongue became established (Liu et al., 2019; Steph et al., 2010). Further single species foraminiferal isotope work is needed to establish whether large isotope gradients were (not) present between Atlantic and Pacific during the OMT (Pearson et al., 1997). Most probably, a combination of temperature and salinity controls best explains the heterogeneous planktonic versus benthic $\delta^{18}O$ signals across the OMT. We note that the differing surface versus deep water response as recorded in planktonic and benthic $\delta^{18}O$ is not unique to the OMT EEP. Across the mid Miocene climatic transition (MMCT), no $\delta^{18}O$ shift in mixed layer planktonic foraminifera was observed, whilst benthic $\delta^{18}O$ increased by 1‰ (Fox et al., 2021). Both the OMT and MMCT records thus suggest that the EEP was sensitive to water-column-heterogeneous temperature (and salinity) variations. The somewhat attenuated expression of the OMT in the *O. umbonatus* $\delta^{18}O$ record is less easily explained, as this species would have experienced a similar drop in bottom water temperatures as *C. mundulus*.

The remarkable increase in the range of variability in the *D. venezuelana* $\delta^{18}O$ record during the early Miocene (Figures 8 and 10), is probably not a measure of increased seasonality, which is minimal at the tropics. Furthermore, our *D. venezuelana* $\delta^{18}O$ record was measured on multiple specimens, thereby averaging any seasonality signals that may have been recorded in individual foraminifer tests. We hypothesize that the increased range of variability in the early Miocene part of the *D. venezuelana* $\delta^{18}O$ record resulted from greater orbitally paced variability mainly in sea surface salinities linked to (a) enhanced movement of oceanic and atmospheric fronts (Hyeong et al., 2014; McPhaden et al., 2006; Neelin et al., 1998), termed here "Fronts Hypothesis," and the control these fronts exert on the strength of equatorial divergent upwelling, and/or (b), perhaps, the amount of salt transported from the Atlantic to the Pacific (Figures 1 and 2), through the CAS (Figure 3), termed here "CAS Hypothesis."

According to the "Fronts Hypothesis," the increased range of *D. venezuelana* $\delta^{18}O$ variability in the early Miocene (Figures 8 and 10) was governed by greater variability of surface currents over Site U1334. The EEP is marked by a complex oceanographic setting, and by considerable salinity gradients between the cold tongue and surrounding surface waters (Figure 1). Furthermore, with 1 psu of salinity change causing ~0.50‰ change in foraminiferal $\delta^{18}O$, versus 1°C temperature change equating to ~0.25‰ change in foraminiferal $\delta^{18}O$, the

movement of surface currents with variable salinities has a greater influence than temperature on foraminiferal $\delta^{18}O$. A change in oceanic frontal systems, is supported by a more permanent southward shift of the ITCZ in response to NH cooling during the OMT (Hyeong et al., 2014). ITCZ changes are closely linked to ENSO intensity/variability, and both processes, in turn, govern the ratio between evaporation and precipitation over the EEP. Lastly, atmospheric, and oceanic fronts control the (variable) strength of equatorial upwelling of colder and more saline intermediate and deep waters (Figures 1 and 2). The Southern Ocean is the source of waters upwelled in the EEP (Schmitz Jr., 1995; Toggweiler et al., 1991), thereby temperature and nutrient changes around Antarctica have a direct impact on the Pacific equatorial region. Furthermore, southern hemisphere cooling and ice growth would impact meridional gradients and cause adjustments to wind patterns and oceanic fronts in the EEP. The shifts in frontal arrangements and/or intensified upwelling in the EEP would result in shifts in upper ocean salinity and temperature. During the early Miocene, rapidly changing frontal system therefore may also have affected planktonic $\delta^{18}O$ values indirectly, through a control on upwelling. However, a modern-like cold-tongue did probably not evolve until the CAS became much more restricted during the latest Miocene or Pliocene (Haug et al., 2001; Liu et al., 2019; Steph et al., 2010).

According to the "CAS Hypothesis," the increased range of *D. venezuelana* $\delta^{18}O$ variability in the early Miocene (Figures 8 and 10), was also predominantly salinity controlled. However, for this hypothesis we speculate that the flow direction and amount exchange of waters between the Atlantic and Pacific (Fraass et al., 2019; von der Heydt & Dijkstra, 2005, 2006), may have become variable on orbital timescales during the early Miocene, and perhaps glacioeustacy controlled, after global mean sea levels were lowered during the peak of the OMT, and other 405 Kyr eccentricity paced global cooling events. However, for this mechanism to be feasible, the CAS would have to be quite restricted already; a requirement that is not currently testable given the best available paleogeographic reconstructions. These suggest a very wide range of potential plate polygon configurations during the OMT (Figure 3), making any physical and chemical oceanographic interpretations (Figure 2) for the OMT highly speculative at best. Overall, the complex interplay between oceanic and atmospheric frontal systems, their effect on surface currents (through the CAS or not), and more speculatively upwelling and (proto-) cold tongue (Liu et al., 2019; Steph et al., 2010), are thought to have become more dynamic during the early Miocene, as documented in the greater range of variability in *D. venezuelana* $\delta^{18}O$ values.

4.4. Global Carbon Cycle and Oceanographic Controls on Foraminiferal $\delta^{13}C$

Like the interpretation of foraminiferal $\delta^{18}O$, absolute offsets between species-specific $\delta^{13}C$ records can be explained by ambient $\delta^{13}C$ of the water mass/pore waters of calcification, between-species differences in respiration, and/or the presence of photosymbionts (Beasley et al., 2021; Beltran et al., 2014; Gasperi & Kennett, 1993; Nederbragt, 2023; Pearson & Wade, 2009; Pearson et al., 1997; Wade & Palike, 2004). However, different long-term trendlines as well as between-record variability on shorter, orbital time scales, require explanations in terms of varying responses to (global) carbon cycle events and/or the imprint of ambient physical and chemical oceanographic conditions that varied throughout the water/sediment column. Our *D. venezuelana* $\delta^{13}C$ record reveals that the CM-OM, previously described from benthic foraminiferal records, also affected the carbon isotope budget of the sub-surface Pacific Ocean, providing further evidence that this event was a major Cenozoic global carbon cycle perturbation. Corroborating evidence for the global nature of CM-OM comes from the similarity in expression of the CM-OM in benthic foraminiferal $\delta^{13}C$ records from the Atlantic Ocean (Billups et al., 2004; Liebrand et al., 2016; Paul et al., 2000). Previous studies have indicated that the CM-OM is probably in response to global cooling across the OMT (Zachos et al., 2001), and linked to the deposition of organic carbon (i.e., ^{12}C) rich deposits and phosphogenesis in shallow marine/shelf environments in Florida and South Africa (Compton et al., 1990, 1993, 2004; Hodell & Woodruff, 1994), which would have resulted in a more ^{12}C depleted global ocean (Figures 9 and 10).

Superimposed on the long-term positive trend in all $\delta^{13}C$ values associated with the CM-OM, we observe a gradually increasing gradient between surface and deep ocean foraminifer species. We use the difference in foraminiferal $\delta^{13}C$, between the asymbiotic deep thermocline-dweller *D. venezuelana* $\delta^{13}C$ and the benthic foraminifer *C. mundulus*, as a means of estimating the strength of the BCP (Figure 11). Our definition of the BCP includes the biologically mediated transfer of carbon from the atmosphere and surface ocean to the deep ocean but excludes the transfer to the sediment. Furthermore, it incorporates the organic carbon pump (i.e., the sinking of particulate organic matter) and the carbonate counter pump (i.e., the remineralization of carbonate in the deep sea). The active removal of ^{12}C from the surface ocean to the deep by biota (Boyle, 1988; Hodell

et al., 2003; Rohling & Cooke, 1999; Toggweiler, 1999), leaves the surface reservoir depleted in the ^{12}C, and the deep reservoir enriched in ^{12}C, causing a gradient between planktonic and benthic $\delta^{13}C$ signals (Kroopnick, 1974). We interpret the BCP to function more effectively, when this gradient is increased, as we document at Site U1334 at, for example, 22.3 Ma (Figure 11). Vice versa, we interpret collapses in vertical $\delta^{13}C$ gradients, for example, at 24.1, 23.7, and 22.1 Ma, as indicative of a (much) less efficient BCP. An increase in primary productivity can cause a more effective BCP. However, the BCP is also temperature dependent (Boscolo-Galazzo et al., 2021), for example, when global climate transitioned to cooler, more glaciated conditions across the OMT. Both processes, that is, increased primary productivity and cooling, were probably at play in the EEP. The overall rise in planktonic $\delta^{13}C$ through our record, coupled with a larger vertical $\delta^{13}C$ gradient, indicates greater productivity in the EEP with enhanced export productivity to the seafloor, perhaps due to upwelling intensity as indicated in the highly variable $\delta^{18}O$ record. The slight cooling of thermocline waters in the early Miocene allowed a greater $\delta^{13}C$ gradient and more particulate organic carbon to reach the seafloor. In the latest Oligocene gradients were generally smaller indicating most or all particulate organic carbon was utilized higher in the water column. Regional cooling of the EEP (in response to eccentricity paced global cooling) is documented in the *D. venezuelana* $\delta^{18}O$ record. Evidence for increased primary productivity comes from the correlation between increased $\delta^{13}C$ gradients and $CaCO_3$ content of the sediment (Figure 11) (Wade & Palike, 2004). We also note that PFARs (Figure 6) were generally highest during 405 Kyr eccentricity minima, concurrent with the highest $\delta^{13}C$ gradients, thereby providing further corroborating evidence for a (partial) primary productivity control on these gradients. Intensification of atmospheric circulation patterns and dust transport from the Eurasia continent eastward to the EEP (Hyeong et al., 2014) could have provided more Fe to an otherwise oligotrophic ocean, thereby increasing primary productivity during the early Miocene, especially during 405 Kyr eccentricity minima, when global climate cooled even further. Cooling at the poles also affects the strength of upwelling in the equatorial upwelling zone, which in turn resulted in an increased nutrient availability, higher primary productivity, an enhanced BCP efficacy, and an increased surface to deep ocean $\delta^{13}C$ gradient (Figures 9 and 11).

5. Conclusions

We present planktonic foraminiferal $\delta^{18}O$ and $\delta^{13}C$ data from Site U1334 located in the EEP that span the late Oligocene and early Miocene time interval (from 24.15 to 21.95 Ma). We juxtapose these planktonic data to previously published benthic foraminiferal $\delta^{18}O$ and $\delta^{13}C$ records from the same site to investigate vertical water column variability in physical and chemical oceanographic conditions. Furthermore, we use these data to describe the evolution of linear trends and long-periodic orbital variability of climate and carbon cycling across the OMT. The uncertainties concerning (a) the many physical, chemical, and biological processes that affected the planktonic and benthic foraminiferal isotope values, and (b) the climatic, cryospheric, and geographic (e.g., the size, depth, and shape of the CAS) background hamper straightforward proxy interpretations. However, we argue that with an open CAS, and hence, a greater flow of salinity from the Atlantic to the Pacific, that salinity influenced the $\delta^{18}O$ of seawater in the EEP, especially during the early Miocene when *D. venezuelana* $\delta^{18}O$ variability drastically increased compared to the late Oligocene. Alternatively, the onset of a more variable movement of surface currents and oceanic fronts across the OMT, would have caused greater salinity variability during the early Miocene. The CM-OM is marked in both surface and deep $\delta^{13}C$ data, supporting that this was a carbon cycle reorganization of global impact with an onset that broadly coincided with the transient global cooling and partially transient (Antarctic) land-ice sheet expansion during the OMT. Increased gradients between surface and deep ocean $\delta^{13}C$ are indicative of an enhanced primary productivity, BCP, and export productivity, forced by enhanced dust delivery through changes in atmospheric circulation, and/or enhanced upwelling of nutrient rich waters during the early Miocene. These gradients were generally best expressed during eccentricity minima, indicating that astronomically forced climate changes modulated BCP intensity in the EEP. Our study further constrains the role of the EEP in contributing and responding to global climate-cryosphere and carbon cycle changes across the OMT.

Conflict of Interest

The authors declare no conflicts of interest relevant to this study.

Data Availability Statement

All data is made available through https://pangaea.de (Liebrand et al., 2024a, 2024b).

Acknowledgments
Samples were provided by the Integrated Ocean Drilling Program, sponsored by the U.S. National Science Foundation and participating countries. We thank Dominika Kasjaniuk, Arnold van Dijk, Maxim Krasnoperov and Jan Drenth for laboratory assistance. We thank Frits Hilgen for useful discussions and/or commenting on an early version of the manuscript. Funding was provided though "Nederlandse Organisatie voor Wetenschappelijk Onderzoek" (NWO) Vici Grant 865.10.001 (H.M.B. and L.J.L), European Research Council (ERC) Grant "Earthsequencing" (D.L., H.P. and A.J.D.), "Deutsche Forschungsgemeinschaft" (DFG) Cluster of Excellence Grant "The Ocean Floor—Earth's Uncharted Interface" (D. L. and H. P.), Natural Environment Research Council (NERC) Grants NE/G014817 and NE/V018361/1, and European Union (EU) Marie Curie "ERAS" (B.S.W.), London NERC Doctoral Training Grant NE/L002485/1 (D. J. K.), a University Research and Leadership Scholarship from the University of Leeds (A.D.H), and ERC Consolidator Grant 771497 (A.S.). H.M.B. conducted the analyses for this study under the program of the Netherlands Earth System Science Centre (NESSC) as part of her PhD research. We thank the associate editor Ursula Röhl and two anonymous reviewers for the valuable feedback they provided during the review stage. We thank Matthew Huber for the editorial handling.

References

Beasley, C., Kender, S., Giosan, L., Bolton, C. T., Anand, P., Leng, M. J., et al. (2021). Evidence of a South Asian proto-monsoon during the Oligocene-Miocene transition. *Paleoceanography and Paleoclimatology*, *36*(9), e2021PA004278. https://doi.org/10.1029/2021PA004278

Beddow, H. M. (2016). *Orbital forcing and climate response (astronomically-tuned age models and stable isotope records for the Oligocene-Miocene). (PhD)* (Vol. 106). Utrecht University. Retrieved from https://dspace.library.uu.nl/handle/1874/337470

Beddow, H. M., Liebrand, D., Sluijs, A., Wade, B. S., & Lourens, L. J. (2016). Global change across the Oligocene-Miocene transition: High-resolution stable isotope records from IODP Site U1334 (equatorial Pacific Ocean). *Paleoceanography*, *31*(1), 81–97. https://doi.org/10.1002/2015pa002820

Beddow, H. M., Liebrand, D., Wilson, D. S., Hilgen, F. J., Sluijs, A., Wade, B. S., & Lourens, L. J. (2018). Astronomical tunings of the Oligocene-Miocene transition from Pacific Ocean Site U1334 and implications for the carbon cycle. *Climate of the Past*, *14*(3), 255–270. https://doi.org/10.5194/cp-14-255-2018

Beltran, C., Rousselle, G., Backman, J., Wade, B. S., & Sicre, M. A. (2014). Paleoenvironmental conditions for the development of calcareous nannofossil acme during the late Miocene in the eastern equatorial Pacific. *Paleoceanography*, *29*(3), 210–222. https://doi.org/10.1002/2013pa002506

Billups, K., Channell, J. E. T., & Zachos, J. (2002). Late Oligocene to early Miocene geochronology and paleoceanography from the subantarctic South Atlantic. *Paleoceanography*, *17*(1), 4-1–4-11. https://doi.org/10.1029/2000PA000568

Billups, K., Palike, H., Channell, J. E. T., Zachos, J. C., & Shackleton, N. J. (2004). Astronomic calibration of the late Oligocene through early Miocene geomagnetic polarity time scale. *Earth and Planetary Science Letters*, *224*(1–2), 33–44. https://doi.org/10.1016/j.epsl.2004.05.004

Bolton, C. T., Lawrence, K. T., Gibbs, S. J., Wilson, P. A., & Herbert, T. D. (2011). Biotic and geochemical evidence for a global latitudinal shift in ocean biogeochemistry and export productivity during the late Pliocene. *Earth and Planetary Science Letters*, *308*(1–2), 200–210. https://doi.org/10.1016/j.epsl.2011.05.046

Boscolo-Galazzo, F., Crichton, K. A., Ridgwell, A., Mawbey, E. M., Wade, B. S., & Pearson, P. N. (2021). Temperature controls carbon cycling and biological evolution in the ocean twilight zone. *Science*, *371*(6534), 1148–1152. https://doi.org/10.1126/science.abb6643

Boyer, T. P., Garcia, H. E., Locarnini, R. A., Zweng, M. M., Hishonov, A. V., Reagan, J. R., et al. (2018). World Ocean Atlas 2018 [Dataset]. Retrieved from https://www.ncei.noaa.gov/access/metadata/landing-page/bin/iso?id=gov.noaa.nodc:NCEI-WOA18

Boyle, E. A. (1988). The role of vertical chemical fractionation in controlling Late Quaternary atmospheric carbon-dioxide. *Journal of Geophysical Research*, *93*(C12), 15701–15714. https://doi.org/10.1029/jc093ic12p15701

Cande, S. C., & Kent, D. V. (1992). A new geomagnetic polarity time scale for the Late Cretaceous and Cenozoic. *Journal of Geophysical Research*, *97*(B10), 13917–13951. https://doi.org/10.1029/92jb01202

Cao, W., Zahirovic, S., Flament, N., Williams, S., Golonka, J., & Müller, R. D. (2017). Improving global paleogeography since the late Paleozoic using paleobiology. *Biogeosciences*, *14*(23), 5425–5439. https://doi.org/10.5194/bg-14-5425-2017

Compton, J. S., Hodell, D. A., Garrido, J. R., & Mallinson, D. J. (1993). Origin and age of phophorite from the south-central Florida Platform: Relation of phosphogenesis to sea-level fluctuations and $\delta^{13}C$ excursions. *Geochimica et Cosmochimica Acta*, *57*(1), 131–146. https://doi.org/10.1016/0016-7037(93)90474-b

Compton, J. S., Snyder, S. W., & Hodell, D. A. (1990). Phosphogenesis and weathering of shelf sediments from the southeastern United States: Implications for Miocene $\delta^{13}C$ excursions and global cooling. *Geology*, *18*(12), 1227–1230. https://doi.org/10.1130/0091-7613(1990)018<1227:pawoss>2.3.co;2

Compton, J. S., Wigley, R., & McMillan, I. K. (2004). Late Cenozoic phosphogenesis on the western shelf of South Africa in the vicinity of the Cape Canyon. *Marine Geology*, *206*(1–4), 19–40. https://doi.org/10.1016/j.margeo.2004.02.004

Cornec, M., Claustre, H., Mignot, A., Guidi, L., Lacour, L., Poteau, A., et al. (2021). Deep chlorophyll maxima in the global ocean: Occurrences, drivers and characteristics. *Global Biogeochemical Cycles*, *35*(4), e2020GB006759. https://doi.org/10.1029/2020GB006759

DeConto, R. M., Pollard, D., Wilson, P. A., Palike, H., Lear, C. H., & Pagani, M. (2008). Thresholds for Cenozoic bipolar glaciation. *Nature*, *455*(7213), 652–U652. https://doi.org/10.1038/nature07337

Diester-Haass, L., Billups, K., & Emeis, K. (2011). Enhanced paleoproductivity across the Oligocene/Miocene boundary as evidenced by benthic foraminiferal accumulation rates. *Palaeogeography, Palaeoclimatology, Palaeoecology*, *302*(3–4), 464–473. https://doi.org/10.1016/j.palaeo.2011.02.006

Edinger, E. N., & Risk, M. J. (1994). Oligocene-Miocene extinction and geographic restriction of Caribbean corals: Roles of turbidity, temperature, and nutrients. *PALAIOS*, *9*(6), 576–598. https://doi.org/10.2307/3515129

Feely, R. A., Wanninkhof, R., Takahashi, T., & Tans, P. (1999). Influence of El Nino on the equatorial Pacific contribution to atmospheric CO_2 accumulation. *Nature*, *398*(6728), 597–601. https://doi.org/10.1038/19273

Ford, H. L., Ravelo, A. C., & Hovan, S. (2012). A deep eastern equatorial Pacific thermocline during the early Pliocene warm period. *Earth and Planetary Science Letters*, *355–356*, 152–161. https://doi.org/10.1016/j.epsl.2012.08.027

Fox, L. R., & Wade, B. S. (2013). Systematic taxonomy of early-middle Miocene planktonic foraminifera from the equatorial Pacific Ocean: Integrated Ocean Drilling Program, Site U1338. *Journal of Foraminiferal Research*, *43*(4), 374–405. https://doi.org/10.2113/gsjfr.43.4.374

Fox, L. R., Wade, B. S., Holbourn, A., Leng, M. J., & Bhatia, R. (2021). Temperature gradients across the Pacific Ocean during the middle Miocene. *Paleoceanography and Paleoclimatology*, *36*(6), e2020PA003924. https://doi.org/10.1029/2020PA003924

Fraass, A. J., Leckie, R. M., Lowery, C. M., & DeConto, R. (2019). Precision in biostratigraphy: Evidence for a temporary flow reversal in the Central American Seaway during or after the Oligocene-Miocene transition. *Journal of Foraminiferal Research*, *49*(4), 357–366. https://doi.org/10.2113/gsjfr.49.4.357

Gallagher, S. J., Auer, G., Brierley, C. M., Fulthorpe, C. S., & Hall, R. (2024). Cenozoic history of the Indonesian Gateway. *Annual Review of Earth and Planetary Sciences*, *52*(1). https://doi.org/10.1146/annurev-earth-040722-111322

Gasperi, J. T., & Kennett, J. P. (1993). Vertical thermal structure evolution of Miocene surface waters—Western equatorial Pacific Dsdp Site-289. *Marine Micropaleontology*, *22*(3), 235–254. https://doi.org/10.1016/0377-8398(93)90046-z

Greenop, R., Sosdian, S. M., Henehan, M. J., Wilson, P. A., Lear, C. H., & Foster, G. L. (2019). Orbital forcing, ice volume, and CO_2 across the Oligocene-Miocene transition. *Paleoceanography and Paleoclimatology*, *34*(3), 316–328. https://doi.org/10.1029/2018PA003420

Haug, G. H., Tiedemann, R., Zahn, R., & Ravelo, A. C. (2001). Role of Panama uplift on oceanic freshwater balance. *Geology*, *29*(3), 207–210. https://doi.org/10.1130/0091-7613(2001)029<0207:ROPUOO>2.0.CO;2

Hay, W. W., DeConto, R., Wold, C. N., Wilson, K. M., Voigt, S., Schulz, M., et al. (1999). Alternative global cretaceous paleogeography. In E. Barrera, & C. Johnson (Eds.), *The evolution of Cretaceous ocean/climate systems* (Vol. 322, pp. 1–47). Geological Society of America Special Paper. https://doi.org/10.1130/0-8137-2332-9.1

Hilgen, F. J., Lourens, L. J., Pälike, H., Batenburg, S., Bohaty, S., Boulila, S., et al. (2020). Should unit-stratotypes and astrochronozones be formally defined? A dual proposal (including postscriptum). *Newsletters on Stratigraphy*, *53*(1), 19–39. https://doi.org/10.1127/nos/2019/0514

Hodell, D. A., Venz, K. A., Charles, C. D., & Ninnemann, U. S. (2003). Pleistocene vertical carbon isotope and carbonate gradients in the South Atlantic sector of the Southern Ocean. *Geochemistry, Geophysics, Geosystems*, *4*(1), 1–19. https://doi.org/10.1029/2002gc000367

Hodell, D. A., & Woodruff, F. (1994). Variations in the strontium isotopic ratio of seawater during the Miocene—Stratigraphic and geochemical implications. *Paleoceanography*, *9*(3), 405–426. https://doi.org/10.1029/94pa00292

Hyeong, K., Lee, J., Seo, I., Lee, M. J., Yoo, C. M., & Khim, B. K. (2014). Southward shift of the intertropical convergence zone due to Northern Hemisphere cooling at the Oligocene-Miocene boundary. *Geology*, *42*(8), 667–670. https://doi.org/10.1130/g35664.1

Kennett, J. P., Keller, G., Srinivasan, M. S., & Kennett, J. P. (1985). Miocene planktonic foraminiferal biogeography and paleoceanographic development of the Indo-Pacific region. In *The Miocene ocean: Paleoceanography and biogeography* (Vol. 163, pp. 0–236). Geological Society of America. https://doi.org/10.1130/mem163-p197

Kim, B., & Zhang, Y. G. (2022). Methane hydrate dissociation across the Oligocene–Miocene boundary. *Nature Geoscience*, *15*(3), 203–209. https://doi.org/10.1038/s41561-022-00895-5

Kroopnick, P. (1974). The dissolved O_2-CO_2-^{13}C system in the eastern equatorial Pacific. *Deep-Sea Research and Oceanographic Abstracts*, *21*(3), 211–227. https://doi.org/10.1016/0011-7471(74)90059-x

Lauvset, S. K., Lange, N., Tanhua, T., Bittig, H. C., Olsen, A., Kozyr, A., et al. (2022). GLODAPv2.2022: The latest version of the global interior ocean biogeochemical data product. *Earth System Science Data*, *14*(12), 5543–5572. https://doi.org/10.5194/essd-14-5543-2022

Lear, C. H., Rosenthal, Y., Coxall, H. K., & Wilson, P. A. (2004). Late Eocene to early Miocene ice sheet dynamics and the global carbon cycle. *Paleoceanography*, *19*(4). https://doi.org/10.1029/2004pa001039

Leckie, R. M., Wade, B. S., Pearson, P. N., Fraass, A. J., King, D. J., Olsson, R. K., et al. (2018). Taxonomy, biostratigraphy, and phylogeny of Oligocene and early Miocene *Paragloboratalia* and *Parasubbotina*. In B. S. Wade, R. K. Olsson, P. N. Pearson, B. T. Huber, & W. A. Berggren (Eds.), *Atlas of Oligocene planktonic foraminifera* (Vol. 46, pp. 125–178). Cushman Foundation. Retrieved from https://www.ucl.ac.uk/earth-sciences/sites/earth_sciences/files/Chapter_5.pdf

Liebrand, D., Beddow, H. M., Lourens, L. J., Palike, H., Raffi, I., Bohaty, S. M., et al. (2016). Cyclostratigraphy and eccentricity tuning of the early Oligocene through early Miocene (30.1-17.1 Ma): Cibicides mundulus stable oxygen and carbon isotope records from Walvis Ridge Site 1264. *Earth and Planetary Science Letters*, *450*, 392–405. https://doi.org/10.1016/j.epsl.2016.06.007

Liebrand, D., de Bakker, A. T. M., Beddow, H. M., Wilson, P. A., Bohaty, S. M., Ruessink, G., et al. (2017). Evolution of the early Antarctic ice ages. *Proceedings of the National Academy of Sciences of the United States of America*, *114*(15), 3867–3872. https://doi.org/10.1073/pnas.1615440114

Liebrand, D., Wade, B. S., Beddow, H. M., King, D., Harrison, A., Johnstone, H. J. H., et al. (2024a). Magnetic susceptibility and calcium carbonate content at the IODP site 320-U1334 [Dataset]. *PANGAEA*. https://doi.org/10.1594/PANGAEA.967473

Liebrand, D., Wade, B. S., Beddow, H. M., King, D., Harrison, A., Johnstone, H. J. H., et al. (2024b). Planktonic foraminifera counts and their oxygen and carbon isotopes at the IODP site 320-U1334. [Dataset]. *PANGAEA*. https://doi.org/10.1594/PANGAEA.967480

Liu, J., Tian, J., Liu, Z., Herbert, T. D., Fedorov, A. V., & Lyle, M. (2019). Eastern equatorial Pacific cold tongue evolution since the late Miocene linked to extratropical climate. *Science Advances*, *5*(4), eaau6060. https://doi.org/10.1126/sciadv.aau6060

Lyle, M., Barron, J., Bralower, T. J., Huber, M., Lyle, A. O., Ravelo, A. C., et al. (2008). Pacific Ocean and Cenozoic evolution of climate. *Reviews of Geophysics*, *46*(2). https://doi.org/10.1029/2005rg000190

Lyle, M., Wilson, P. A., Janecek, T. R., & Al, E. (2002). *Proceedings of the Ocean Drilling Program, Initial Reports, 199: College Station, TX (Ocean Drilling Program)*. https://doi.org/10.2973/odp.proc.ir.199.2002

Ma, Z., Ravelo, A. C., Liu, Z., Zhou, L., & Paytan, A. (2015). Export production fluctuations in the eastern equatorial Pacific during the Pliocene-Pleistocene: Reconstruction using barite accumulation rates. *Paleoceanography*, *30*(11), 1455–1469. https://doi.org/10.1002/2015pa002860

Marron, J. S., & Zhang, J.-T. (2005). SiZer for smoothing splines. *Computational Statistics*, *20*(3), 481–502. https://doi.org/10.1007/bf02741310

Matsui, H., Nishi, H., Takashima, R., Kuroyanagi, A., Ikehara, M., Takayanagi, H., & Iryu, Y. (2016). Changes in the depth habitat of the Oligocene planktic foraminifera (*Dentoglobigerina venezuelana*) induced by thermocline deepening in the eastern equatorial Pacific. *Paleoceanography*, *31*(6), 715–731. https://doi.org/10.1002/2016pa002950

Mawbey, E. M., & Lear, C. H. (2013). Carbon cycle feedbacks during the Oligocene-Miocene transient glaciation. *Geology*, *41*(9), 963–966. https://doi.org/10.1130/g34422.1

McPhaden, M. J., Zebiak, S. E., & Glantz, M. H. (2006). ENSO as an integrating concept in Earth science. *Science*, *314*(5806), 1740–1745. https://doi.org/10.1126/science.1132588

Meckler, A. N., Sexton, P. F., Piasecki, A. M., Leutert, T. J., Marquardt, J., Ziegler, M., et al. (2022). Cenozoic evolution of deep ocean temperature from clumped isotope thermometry. *Science*, *377*(6601), 86–90. https://doi.org/10.1126/science.abk0604

Merdith, A. S., Williams, S. E., Collins, A. S., Tetley, M. G., Mulder, J. A., Blades, M. L., et al. (2021). Extending full-plate tectonic models into deep time: Linking the Neoproterozoic and the Phanerozoic. *Earth-Science Reviews*, *214*, 103477. https://doi.org/10.1016/j.earscirev.2020.103477

Mitchell, N. C., Lyle, M. W., Knappenberger, M. B., & Liberty, L. M. (2003). Lower Miocene to present stratigraphy of the equatorial Pacific sediment bulge and carbonate dissolution anomalies. *Paleoceanography*, *18*(2), 1038. https://doi.org/10.1029/2002pa000828

Montes, C., Bayona, G., Cardona, A., Buchs, D. M., Silva, C. A., Morón, S., et al. (2012). Arc-continent collision and orocline formation: Closing of the Central American seaway. *Journal of Geophysical Research*, *117*(B4), B04105. https://doi.org/10.1029/2011JB008959

Moore, T. C., Jr., Backman, J., Raffi, I., Nigrini, C., Sanfilippo, A., Pälike, H., & Lyle, M. (2004). Paleogene tropical Pacific: Clues to circulation, productivity, and plate motion. *Paleoceanography*, *19*(3), PA3013. https://doi.org/10.1029/2003PA000998

Moore, T. C., Wade, B. S., Westerhold, T., Erhardt, A. M., Coxall, H. K., Baldauf, J., & Wagner, M. (2014). Equatorial Pacific productivity changes near the Eocene-Oligocene boundary. *Paleoceanography*, *29*(9), 825–844. https://doi.org/10.1002/2014pa002656

Müller, R. D., Cannon, J., Qin, X., Watson, R. J., Gurnis, M., Williams, S., et al. (2018). GPlates: Building a virtual Earth through deep time. *Geochemistry, Geophysics, Geosystems*, *19*(7), 2243–2261. https://doi.org/10.1029/2018gc007584

Nederbragt, A. J. (2023). The effect of seawater carbonate chemistry on the stable isotope composition of *Cibicidoides wuellerstorfi* and other *Cibicidoides* species. *Paleoceanography and Paleoclimatology*, *38*(9), e2023PA004667. https://doi.org/10.1029/2023PA004667

Neelin, J. D., Battisti, D. S., Hirst, A. C., Jin, F.-F., Wakata, Y., Yamagata, T., & Zebiak, S. E. (1998). ENSO theory. *Journal of Geophysical Research*, *103*(C7), 14261–14290. https://doi.org/10.1029/97jc03424

Pälike, H., Frazier, J., & Zachos, J. C. (2006). Extended orbitally forced palaeoclimatic records from the equatorial Atlantic Ceara Rise. *Quaternary Science Reviews*, *25*(23–24), 3138–3149. https://doi.org/10.1016/j.quascirev.2006.02.011

Pälike, H., Lyle, M. W., Nishi, H., & Al, E. (2012). A Cenozoic record of the equatorial Pacific carbonate compensation depth. *Nature*, *488*, 609–615. https://doi.org/10.1038/nature11360

Pälike, H., Lyle, M., Nishi, H., Raffi, I., Gamage, K., Klaus, A., & the Expedition 320/321 Scientists. (2010). *Proceedings of the Integrated Ocean Drilling Program, 320/321: Tokyo (Integrated Ocean Drilling Program Management International, Inc.)*. https://doi.org/10.2204/iodp.proc.320321.2010

Paul, H. A., Zachos, J. C., Flower, B. P., & Tripati, A. (2000). Orbitally induced climate and geochemical variability across the Oligocene/Miocene boundary. *Paleoceanography*, *15*(5), 471–485. https://doi.org/10.1029/1999pa000443

Pearson, P. N. (2012). Oxygen isotopes in foraminifera: Overview and historical review. In L. Ivany, & B. T. Huber (Eds.), *Reconstructing Earth's deep-time climate: The state-of-the-art in 2012: Paleontological society short course* (Vol. 18, pp. 1–38). https://doi.org/10.1017/s1089332600002539

Pearson, P. N., Ditchfield, P. W., Singano, J., Harcourt-Brown, K. G., Nicholas, C. J., Olsson, R. K., et al. (2001). Warm tropical sea surface temperatures in the Late Cretaceous and Eocene epochs. *Nature*, *413*(6855), 481–487. https://doi.org/10.1038/35097000

Pearson, P. N., Shackleton, N. J., Weedon, G. P., & Hall, M. A. (1997). Multispecies planktonic foraminifer stable isotope stratigraphy through Oligocene/Miocene boundary climatic cycles, Site 926. In *Vol. 154. Proceedings of the Ocean Drilling Program, Scientific Results*. Retrieved from http://www-odp.tamu.edu/publications/154_SR/29_CHAP.PDF

Pearson, P. N., & Wade, B. S. (2009). Taxonomy and stable isotope paleoecology of well-preserved planktonic foraminifera from the uppermost Oligocene of Trinidad. *Journal of Foraminiferal Research*, *39*(3), 191–217. https://doi.org/10.2113/gsjfr.39.3.191

Rae, J. W. B., Zhang, Y. G., Liu, X., Foster, G. L., Stoll, H. M., & Whiteford, R. D. M. (2021). Atmospheric CO_2 over the past 66 million years from marine archives. *Annual Review of Earth and Planetary Sciences*, *49*(1), 609–641. https://doi.org/10.1146/annurev-earth-082420-063026

Rippert, N., Max, L., Mackensen, A., Cacho, I., Povea, P., & Tiedemann, R. (2017). Alternating influence of northern versus southern-sourced water masses on the equatorial Pacific subthermocline during the past 240 ka. *Paleoceanography*, *32*(11), 1256–1274. https://doi.org/10.1002/2017pa003133

Rohling, E. J., & Cooke, S. (1999). Stable oxygen and carbon isotopes in foraminiferal carbonate shells. In K. Barum, & S. Gupta (Eds.), *Modern foraminifera*. Springer. https://doi.org/10.1007/0-306-48104-9_14

Schlitzer, R. (2022). Ocean data View: odv.awi.de [Software]. Retrieved from https://odv.awi.de/

Schmitz, W. J., Jr. (1995). On the interbasin-scale thermohaline circulation. *Reviews of Geophysics*, *33*(2), 151–173. https://doi.org/10.1029/95RG00879

Sexton, P. F., Wilson, P. A., & Pearson, P. N. (2006). Microstructural and geochemical perspectives on planktic foraminiferal preservation: "Glassy" versus "Frosty". *Geochemistry, Geophysics, Geosystems*, *7*(12), Q12P19. https://doi.org/10.1029/2006GC001291

Spezzaferri, S., Kucera, M., Pearson, P. N., Wade, B. S., Rappo, S., Poole, C. R., et al. (2015). Fossil and genetic evidence for the polyphyletic nature of the planktonic foraminifera "*Globigerinoides*", and description of the New Genus *Trilobatus*. *PLoS One*, *10*(5), e0128108. https://doi.org/10.1371/journal.pone.0128108

Spezzaferri, S., Olsson, R. K., & Hemleben, C. (2018). Taxonomy, biostratigraphy, and phylogeny of Oligocene to lower Miocene *Globigerinoides* and *Trilobatus*. In B. S. Wade, R. K. Olsson, P. N. Pearson, B. T. Huber, & W. A. Berggren (Eds.), *Atlas of Oligocene planktonic foraminifera* (Vol. 46, pp. 269–306). Cushman Foundation Special Publication. Retrieved from https://pubs.geoscienceworld.org/cushmanfoundation/books/book/2271/chapter-abstract/126275371/TAXONOMY-BIOSTRATIGRAPHY-AND-PHYLOGENY-OF?redirectedFrom=fulltext

Steinthorsdottir, M., Coxall, H. K., de Boer, A. M., Huber, M., Barbolini, N., Bradshaw, C. D., et al. (2021). The Miocene: The future of the past. *Paleoceanography and Paleoclimatology*, *36*(4), e2020PA004037. https://doi.org/10.1029/2020PA004037

Steph, S., Tiedemann, R., Prange, M., Groeneveld, J., Schulz, M., Timmermann, A., et al. (2010). Early Pliocene increase in thermohaline overturning: A precondition for the development of the modern equatorial Pacific cold tongue. *Paleoceanography*, *25*(2), PA2202. https://doi.org/10.1029/2008PA001645

Stewart, J. A., Wilson, P. A., Edgar, K. M., Anand, P., & James, R. H. (2012). Geochemical assessment of the palaeoecology, ontogeny, morphotypic variability and palaeoceanographic utility of "Dentoglobigerina" venezuelana. *Marine Micropaleontology*, *84–85*, 74–86. https://doi.org/10.1016/j.marmicro.2011.11.003

Takahashi, T., Sutherland, S. C., Sweeney, C., Poisson, A., Metzl, N., Tilbrook, B., et al. (2002). Global sea-air CO_2 flux based on climatological surface ocean pCO_2, and seasonal biological and temperature effects. *Deep-Sea Research Part II-Topical Studies in Oceanography*, *49*(9–10), 1601–1622. https://doi.org/10.1016/s0967-0645(02)00003-6

Toggweiler, J. R. (1999). Variation of atmospheric CO_2 by ventilation of the ocean's deepest water. *Paleoceanography*, *14*(5), 571–588. https://doi.org/10.1029/1999pa900033

Toggweiler, J. R., Dixon, K., & Broecker, W. S. (1991). The Peru upwelling and the ventilation of the South Pacific thermocline. *Journal of Geophysical Research*, *96*(C11), 20467–20497. https://doi.org/10.1029/91JC02063

von der Heydt, A., & Dijkstra, H. A. (2005). Flow reorganizations in the Panama Seaway: A cause for the demise of Miocene corals? *Geophysical Research Letters*, *32*(2), L02609. https://doi.org/10.1029/2004gl020990

von der Heydt, A., & Dijkstra, H. A. (2006). Effect of ocean gateways on the global ocean circulation in the late Oligocene and early Miocene. *Paleoceanography*, *1*, PA1011. https://doi.org/10.1029/2005PA001149

Wade, B. S., Berggren, W. A., & Olsson, R. K. (2007). The biostratigraphy and paleobiology of Oligocene planktonic foraminifera from the equatorial Pacific Ocean (ODP Site 1218). *Marine Micropaleontology*, *62*(3), 167–179. https://doi.org/10.1016/j.marmicro.2006.08.005

Wade, B. S., O'Neill, J. F., Phujareanchaiwon, C., Ali, I., Lyle, M., & Witkowski, J. (2020). Evolution of deep-sea sediments across the Paleocene-Eocene and Eocene-Oligocene boundaries. *Earth-Science Reviews*, *211*, 103403. https://doi.org/10.1016/j.earscirev.2020.103403

Wade, B. S., & Palike, H. (2004). Oligocene climate dynamics. *Paleoceanography*, *19*(4), PA4019. https://doi.org/10.1029/2004pa001042

Wade, B. S., Pearson, P. N., Berggren, W. A., & Pälike, H. (2011). Review and revision of Cenozoic tropical planktonic foraminiferal biostratigraphy and calibration to the geomagnetic polarity and astronomical time scale. *Earth-Science Reviews*, *104*(1), 111–142. https://doi.org/10.1016/j.earscirev.2010.09.003

Wade, B. S., Pearson, P. N., Olsson, R. K., Fraass, A. J., Leckie, R. M., & Hemleben, C. (2018). Taxonomy, biostratigraphy, and phylogeny of Oligocene and lower Miocene *Dentoglobigerina* and *Globoquadrina*. In B. S. Wade, R. K. Olsson, P. N. Pearson, B. T. Huber, & W. A. Berggren (Eds.), *Atlas of Oligocene planktonic foraminifera* (Vol. 46, pp. 331–384). Cushman Foundation. Retrieved from https://pubs.

geoscienceworld.org/cushmanfoundation/books/book/2271/chapter-abstract/126275375/TAXONOMY-BIOSTRATIGRAPHY-AND-PHYLOGENY-OF?redirectedFrom=fulltext

Wang, X., Christian, J. R., Murtugudde, R., & Busalacchi, A. J. (2005). Ecosystem dynamics and export production in the central and eastern equatorial Pacific: A modeling study of impact of ENSO. *Geophysical Research Letters*, *32*(2), L02608. https://doi.org/10.1029/2004GL021538

Westerhold, T., Marwan, N., Drury, A. J., Liebrand, D., Agnini, C., Anagnostou, E., et al. (2020). An astronomically dated record of Earth's climate and its predictability over the last 66 million years. *Science*, *369*(6509), 1383–1387. https://doi.org/10.1126/science.aba6853

Westerhold, T., Röhl, U., & Laskar, J. (2012). Time scale controversy: Accurate orbital calibration of the early Paleogene. *Gechemistry, Geophysics, Geosystems*, *13*(6), Q06015. https://doi.org/10.1029/2012gc004096

Westerhold, T., Röhl, U., Wilkens, R., Pälike, H., Lyle, M., Dunkley Jones, T., et al. (2012). Revised composite depth scales and integration of IODP Sites U1331-U1334 and ODP Sites 1218-1220. In *Proceedings of the Integrated Ocean Drilling Program* (pp. 320–321). https://doi.org/10.2204/iodp.proc.320321.201.2012

Wyrtki, K. (1981). An estimate of equatorial upwelling in the Pacific. *Journal of Physical Oceanography*, *11*(9), 1205–1214. https://doi.org/10.1175/1520-0485(1981)011<1205:aeoeui>2.0.co;2

Zachariasse, W. J., & Sudijono (2012). New data on the morphology and classification of the Oligocene-Miocene planktonic foraminifer *Paragloboratalia siakensis* (Leroy, 1939). *Journal of Foraminiferal Research*, *42*(2), 156–168. https://doi.org/10.2113/gsjfr.42.2.156

Zachos, J. C., Shackleton, N. J., Revenaugh, J. S., Palike, H., & Flower, B. P. (2001). Climate response to orbital forcing across the Oligocene-Miocene boundary. *Science*, *292*(5515), 274–278. https://doi.org/10.1126/science.1058288